

¹ **High-resolution regional climate model evaluation using variable-resolution**

² **CESM over California**

³ Xingying Huang, * Alan M. Rhoades and Paul A. Ullrich

⁴ *Department of Land, Air and Water Resources, University of California, Davis*

⁵ Colin M. Zarzycki

⁶ *National Center for Atmospheric Research*

⁷ *Corresponding author address: Xingying Huang, Department of Land, Air and Water Resources,

⁸ University of California Davis, Davis, CA 95616.

⁹ E-mail: xyhuang@ucdavis.edu

ABSTRACT

10 Understanding the effect of climate change at regional scales remains a topic
11 of intensive research. Computational constraints have meant that the high hor-
12 izontal resolutions required to reach regional scales have been largely out of
13 reach of modern global climate models. However, high horizontal resolution
14 is needed to represent topographic forcing, which is a significant driver of
15 local climate variability. Although regional climate models (RCMs) have tra-
16 ditionally been used at these scales, variable-resolution global climate mod-
17 els (VRGCMs) have recently arisen as an alternative for studying regional
18 weather and climate. In this paper, the recently developed variable-resolution
19 option within the Community Earth System Model (CESM) is assessed for
20 long-term regional climate modeling. The mean climatology of temperature
21 and precipitation, across California's diverse climate zones, is analyzed and
22 contrasted with the Weather Research and Forcasting (WRF) model (as a tra-
23 ditional RCM), regional reanalysis, gridded observational datasets and uni-
24 form high-resolution CESM with the finite volume (FV) dynamical core. The
25 results show that variable-resolution CESM is competitive in representing re-
26 gional climatology on both annual and seasonal time scales. This assessment
27 adds value to the use of VRGCMs for projecting climate change over the
28 coming century and improve our understanding of both past and future re-
29 gional climate related to fine-scale processes. This assessment is also relevant
30 for addressing the scale limitation of current RCMs or VRGCMs when next-
31 generation model resolution increases to $\sim 10\text{km}$ and beyond.

³² **1. Introduction**

³³ Global climate models (GCMs) have been widely used to simulate both past and future cli-
³⁴ mate. Although GCMs have demonstrated the capability to successfully represent large-scale
³⁵ features of the climate system, they are usually employed at coarse resolutions ($\sim 1^\circ$), largely
³⁶ due to computational limitations. Global climate reanalysis datasets, which assimilate climate
³⁷ observations using a global model, represent a best estimate of historical weather patterns, but
³⁸ still have relatively low resolutions no finer than 0.5° (<http://reanalyses.org/atmosphere/>
³⁹) overview-current-reanalyses). Consequently, regional climate is not well captured by ei-
⁴⁰ ther GCMs or global reanalysis datasets. However, dynamical processes at unrepresented scales
⁴¹ are significant drivers for regional and local climate variability, especially over complex terrain
⁴² (Soares et al. 2012). In order to capture these fine-scale dynamical features, high horizontal reso-
⁴³ lution is needed to allow for a more accurate representation of fine-scale forcings, processes and
⁴⁴ interactions (Leung et al. 2003; Rauscher et al. 2010). We anticipate that with these enhancements
⁴⁵ the regional climate information will be more usable for policy makers and local stakeholders in
⁴⁶ formulating climate adaptation and mitigation strategies.

⁴⁷ In order to model regional climate at high spatial and temporal resolution over a limited area,
⁴⁸ downscaling methods have been developed. There are largely two approaches for downscaling:
⁴⁹ The first is statistical downscaling, which aims to estimate fine scale behavior via analysis of the
⁵⁰ statistical relationships between observed small-scale variables and larger (GCM) scale variables
⁵¹ (Fowler et al. 2007). This method is empirical and cannot be used if the observed relationships
⁵² do not hold with a changing climate (Soares et al. 2012). The second approach is dynamical
⁵³ downscaling, which uses a numerical model to simulate higher spatial resolution conditions in
⁵⁴ greater detail. Dynamical downscaling is popular and commonly employed using nested limited-

area models (LAMs) or by using a variable resolution GCM (VRGCM) to model regional scales (Laprise 2008). In this context, LAMs are typically referred as regional climate models (RCMs) when applied to climate scales. RCMs are forced by output of GCMs or reanalysis data, and have been widely used, particularly to capture physically consistent regional and local circulations at the needed spatial and temporal scales (Christensen et al. 2007; Bukovsky and Karoly 2009; Mearns et al. 2012). Recently, VRGCMs have been increasingly employed for modeling regional climate. This approach uses a global model that includes high-resolution over a specific region and lower resolution over the remainder of the globe (Staniforth and Mitchell 1978; Fox-Rabinovitz et al. 1997). Within VRGCM, there are also different strategies of achieving high-resolution over the area of interest such as stretched-grid models or grid refinement (Fox-Rabinovitz et al. 1997; Zarzycki et al. 2015). VRGCMs have been demonstrated to be effective for regional climate studies and applications, owing to the advantages of traditional GCMs in representing large-scale features, at a reduced computational cost compared to uniform GCMs (Fox-Rabinovitz et al. 2001, 2006; Rauscher et al. 2013; Zarzycki et al. 2014; Zarzycki and Jablonowski 2014; Zarzycki et al. 2015). Fox et al. (2000) found that the stretched-grid version of a GCM simulated not only large-scale but also mesoscale features especially when considering orographic forcing (?).

Compared with RCMs, a key advantage of VRGCMs is that they use a single, unified modeling framework, rather than a separate GCM and RCM. Thus, VRGCMs avoid potential inconsistency between the global and regional domains, and naturally support two-way interaction between these domains without the need for nudging (Warner et al. 1997; McDonald 2003; Laprise et al. 2008; Mesinger and Veljovic 2013). However, in order to obtain deeper insight into the performance of these two modeling approaches, it is necessary to compare them directly. For the purposes of this paper, we will focus on the recently developed variable-resolution Community Earth System Model (varres-CESM) using the grid refinement technique as our VRGCM of interest. Although

79 CESM has been well-used for uniform resolution modeling, variable-resolution in the Commu-
80 nity Atmosphere Models (CAM) Spectral Element (SE) dynamical core has only been recently
81 developed. Zarzycki et al. (2014) applied this option in CAM-SE and showed that high-resolution
82 simulation of topical cyclones represented significant improvements over the unrefined simulation
83 (Zarzycki et al. 2014). Zarzycki et al. also compared the large-scale features of varres-CESM
84 0.25° and uniform CESM at 1 degree, and found that adding refined region over the globe did not
85 affect the global circulation noticeably (Zarzycki and Jablonowski 2014; Zarzycki et al. 2015).

86 However, varres-CESM has yet to be rigorously investigated for long-term regional climate sim-
87 ulation (Taylor and Fournier 2010; Zarzycki et al. 2014). And in this paper, it is the first time to
88 investigate whether VRGCMs can show similar or even better ability in regional climate modeling
89 compared with traditional method of RCMs. Consequently, the goal of this paper is to evaluate
90 the performance of varres-CESM against gridded observational data, reanalysis data and in com-
91 parison to a RCM. Also, outputs from a uniform high-resolution CESM simulation have been
92 utilized here Wehner et al. (2014a). Our variable-resolution simulations will focus on relatively
93 high resolutions for climate assessment, namely 28km and 14km regional resolution, which are
94 much more typical for dynamically downscaled studies. For comparison with the more widely
95 used RCM method, the Weather Research and Forecasting (WRF) model will be used (Skamarock
96 et al. 2005). The study focuses on models' ability to represent current climate statistics, partic-
97 ularly those relative to climate extremes. We anticipate that this assessment will add value in
98 modeling mean regional climatology and improve our understanding about the effects of multi-
99 scale processes in regional climate regulation. Our goal is also to advance the understanding of
100 better use of models in future climate predictions and climatic extremes studies regionally.

101 With its complex topography, coastal influences, and wide latitudinal range, this makes CA an
102 excellent test bed for high-resolution climate studies. Also, an understanding of local climate

variability is incredibly important for policymakers and stakeholders in California due to its vast agricultural industry, wide demographics, and vulnerability to anthropogenically-induced climate change (Hayhoe et al. 2004; Cayan et al. 2008). Existing studies show that RCMs are able to capture physically consistent regional and local circulations at the needed spatial and time scales (Leung et al. 2003; Laprise 2008; ?). RCM simulations over California have also been conducted in previous studies and showed the need of high resolution to better study regional climate and extreme events, especially over complex topography with large climate gradients (Leung et al. 2004; Kanamitsu and Kanamaru 2007; Caldwell et al. 2009; Pan et al. 2011; Pierce et al. 2013). Caldwell et al. (2009), in particular, presented results from WRF (Weather Research and Forecasting) at 12km spatial resolution showing both the overall consistency and some biases between simulations and observations.

This paper is organized as follows. Section 2 describes the model setup, verification data and evaluation methods. In section 3, results are demonstrated focusing on 2 m temperature (Ts) and precipitation (Pr). Key results are summarized along with further discussion in section 4.

2. Models and Methodology

a. Simulation design

All simulations use the AMIP (Atmospheric Model Intercomparison Project) protocols (Gates 1992). AMIP simulations attempt to recreate a climatology similar to that observed over the past few decades. The ocean model is disabled and the model is forced with prescribed sea-surface temperatures (SSTs) and ice concentrations.

123 1) VARRES-CESM

124 CESM is a state-of-the-art Earth modeling framework developed by the National Center for At-
mospheric Research (NCAR), consisting of atmospheric, oceanic, land and sea ice components
125 and has been heavily used for understanding the effects of global climate change (Neale et al.
126 2010a; Hurrell et al. 2013). Different component models are connected by a couple component.
127 In this way, the interfacial states and fluxes between the various component models are commu-
128 nicated and the fluxed quantities are conserved. Since we follow AMIP protocols in this study,
129 communication is mainly occurred between atmospheric and land model. Ocean model and sean
130 ice component are disabled. Here, CAM version 5 (CAM5) (Neale et al. 2010b) and the Com-
131 munity Land Model (CLM) version 4 (Oleson et al. 2010) are used. As mentioned earlier, SE
132 was used as the dynamical core in CAM along with the variable-resolution grid support. The
133 FAMIPC5 (F_AMIP_CAM5) compset was chosen for the simulations as it is the standard protocol
134 for AMIP and is less computationally demanding.

136 For our study, the variable-resolution cubed-sphere grids are generated for use in CAM and CLM
137 with the open-source software package SQuadGen (Ullrich 2014). The grids used are depicted in
138 Figure 2. The maximum horizontal resolution on these grids are 0.25 degree ($\sim 28\text{km}$) and 0.125
139 degree ($\sim 14\text{km}$), with a 1 degree resolution covering the rest of the globe. These resolutions
140 have been selected because CAM-SE naturally supports a 2:1 aspect ratio, meaning there are two
141 transition layers from 1 degree to 0.25 degree, and one additional transition from 0.25 degree to
142 0.125 degree. The meteorological patterns (e.g. wind, pressure and precipitation) showed natural
143 and conserved results over the transition boundary as described in (Zarzycki et al. 2015). The time
144 period is from 1979-01-01 to 2005-12-31 (UTC), and year 1979 was discarded as spin up time for
145 CLM4.0. We chose this time period to present the recent historical climate and try to achieve the

¹⁴⁶ best balance between reproducibility and computational feasibility, which is further discussed in
¹⁴⁷ the Methodology part.

¹⁴⁸ Variable-resolution topography files have been produced by starting with the National Geophys-
¹⁴⁹ ical Data Center (NGDC) 2-min (~ 3.5 km) Gridded Global Relief Dataset (ETOPO2v2) topog-
¹⁵⁰ raphy dataset and applying the differential smoothing technique by adjusting the c parameter from
¹⁵¹ Eq. (1) in Zarzycki et al. (2015). Land surface datasets, and plant functional types, were created at
¹⁵² the standard 0.50 degree resolution. Greenhouse gas (GHG) concentrations are prescribed based
¹⁵³ on historical observations. SSTs and ice coverage are supplied by the 1degree Hadley Centre Sea
¹⁵⁴ Ice and Sea Surface Temperature dataset (HadISST) (Hurrell et al. 2008). Tuning parameters are
¹⁵⁵ not modified from their default configuration.

¹⁵⁶ 2) UNIFORM CESM

¹⁵⁷ Output from a globally uniform CESM run at 0.25° global spatial resolution is utilized for com-
¹⁵⁸ parison. It helps us to see if variable-resolution CESM, which is at much lower computation cost
¹⁵⁹ than uniform one, can show comparable performance in modeling mean climatology (Bacmeister
¹⁶⁰ et al. 2014). This globally uniform simulation uses the CAM5-FV (finite volume) dynamical core
¹⁶¹ and is described in additional detail in Wehner et al. (2014a) and Wehner et al. (2014b). Note that
¹⁶² the appendix of the latter paper lists parameters that are different from the public release. **need to**
¹⁶³ **add details about this and which parameters are different from the public version.**

¹⁶⁴ 3) WRF

¹⁶⁵ WRF has gained wide acceptance in studying regional climate over the past decade, showing
¹⁶⁶ its adequate capability in representation of fine-scale climate properties (Lo et al. 2008; Leung
¹⁶⁷ and Qian 2009; Soares et al. 2012). In this study, the fully compressible non-hydrostatic WRF

model in version 3.5.1 with the Advanced Research WRF (ARW) dynamical solver is used. ERA (ECMWF re-analysis)-Interim surface and pressure-level reanalysis was used to provide initial and lateral conditions for the domains. The lateral conditions and SSTs were updated every 6 hours. ERA-Interim reanalysis (\sim 80 km) has been widely used and validated for its reliability as forcing data (Dee et al. 2011). Two simulations are conducted with horizontal resolution of 27km and 9km simultaneously, over the time period 1979-01-01 to 2005-12-31 (UTC). The year 1979 is used as a spin-up period and is discarded for purposes of analysis. The \sim 10 km resolution is actually finer than most previous studies for long-term climate.

The simulation domains of WRF 9km are depicted in Figure 1. For the WRF 27km simulation, one domain is used. For the WRF 9km simulation, two nested domains are used with the outer domain at 27km (same as the WRF 27km) and inner domain at 9km horizontal grid resolution. As a common way in WRF, two-way nesting is enabled by feeding back information from the fine grid onto the coarse grid, thus the nested region's process of the coarse domain is replaced by the fine grid result (Skamarock and Klemp 2008). These choices have been made to satisfy the natural WRF refinement ratio of 3:1. Both grids are centered on CA and have respectively, 120×110 and 151×172 grid points. Around the boundaries, 10 grid points are used as lateral relaxation zones. In order to reduce the drift between forcing data and RCM, grid nudging (Stauffer and Seaman 1990) was applied to the outer domain every 6 hours at all levels except the planetary boundary layer (PBL) as suggested by Lo et al. (2008). This setup uses 41 vertical levels with model top pressure at 50 hPa. The topography data used in 27km and 9km are interpolated from USGS (U.S. Geological Survey) elevation data with 10m and 2m resolution respectively.

Additionally, we used the following physics parameterizations: WSM (WRF Single-Moment) 6-class graupel microphysics scheme (Hong and Lim 2006), Kain-Fritsch cumulus scheme (Kain 2004), CAM shortwave and longwave radiation schemes (Collins et al. 2004). These settings

192 are supported by the one-year test running result with different options of cumulus scheme and
193 radiation schemes. For the boundary layer, the Yonsei University scheme (YSU) (Hong et al.
194 2006) and the Noah Land Surface Model (Chen and Dudhia 2001) were used. Both were chosen
195 as they are common for climate applications that balance long-term reliability and computational
196 cost.

197 *b. Topography*

198 The grid-scale topography for all simulations is contrasted in Figure 3. The higher resolution
199 simulations provide a much finer representation of regional topography. This is important for
200 understanding local climate since topography is an important driver for fine-scale dynamic pro-
201 cesses, especially over complex terrain. Some differences are also apparent between the 28km
202 varres-CESM and 27km WRF model, particularly over the Central Valley, and indicative of a
203 different methodology for preparation of the topography dataset.

204 *c. Datasets*

205 For validation purpose, available reanalysis and gridded observational datasets of the highest
206 quality are employed (see Table 1). These data products incorporate station measurements or
207 satellite information and other data. Although these products are generally based on observations,
208 they are based on different network of weather stations. And these datasets are scaled and gridded
209 using varied interpolation techniques, elevation model and processing algorithms. In this way,
210 using more reference datasets rather than one is important to account for the uncertainties, for
211 assessing the performance of the WRF and CESM simulations in terms of both mean behavior
212 and variability. Moreover, in this study, our purpose of using these products is to serve as realistic
213 proxies to allow for a comparison of the model results. We acknowledge that reanalysis products

214 are particularly sensitive to model choice and choice of assimilated observations and so cannot be
215 treated as truth. Detailed descriptions of these datasets are as follows.

216 (i) *NARR*: The North American Regional Reanalysis (NARR) (Mesinger et al. 2006) provides
217 dynamically downscaled data over North America at ~ 32 km resolution and 3 hourly intervals
218 from 1979 through present. It is National Centers for Environmental Prediction (NCEP)'s high
219 resolution reanalysis product combined model and assimilated dataset. All major climatological
220 variables are present in NARR, making it an excellent candidate for assessment of regional cli-
221 mate. Nonetheless, some inaccuracies have been identified in NARR that must be accounted for,
222 including deficiencies in precipitation fields away from the continental US (Bukovsky and Karoly
223 2007).

224 (ii) *NCEP CPC*: This data set is CPC unified gauge-based analysis of daily precipitation pro-
225 vided by the National Oceanic and Atmospheric Administration (NOAA) Climate Prediction Cen-
226 ter (CPC). It is a suite of unified precipitation products with consistent and improved quality by
227 combining all information available at CPC and by taking advantage of the optimal interpolation
228 (OI) objective analysis technique. The gauge analysis covers the Conterminous United States on
229 a fine-resolution at 0.25° from 1948/01/01 to 2006/12/3.

230 (iii) *UW*: The UW daily gridded meteorological data is obtained from the Surface Water Mod-
231eling group at the University of Washington (Maurer et al. 2002; Hamlet and Lettenmaier 2005).
232 UW incorporated topographic corrections by forcing the long-term average precipitation to match
233 that of the PRISM dataset. Temperature dataset is produced in a similar fashion as precipitation,
234 but used a simple 6.1 K/km lapse rate for topographic effect. The dataset is at 0.125° horizontal
235 resolution and provided from year 1949 to 2010.

236 (iv) *PRISM*: The Parameter-elevation Regressions on Independent Slopes Model (PRISM) (Daly
237 et al. 2008) supports a 4km gridded dataset obtained by taking wide range of point measurements
238 and applying a weighted regression scheme that accounts for many factors affecting the local cli-
239 matology. The datasets include total precipitation and minimum/maximum, (derived) mean tem-
240 peratures and dewpoints, based on sophisticated quality control measures. Monthly climatological
241 variables are available for 1895 through 2014 provided by the PRISM Climate Group. PRISM is
242 U.S. Department of Agriculture (USDA)'s official climatological data. We will use this product as
243 the main reference dataset for model assessment.

244 (v) *Daymet*: Daymet is an extremely high resolution (1 km) gridded dataset with daily outputs
245 of total precipitation, humidity, and minimum/maximum temperature covering the years of 1980
246 through 2013 (Thornton et al. 1997; Thornton and Running 1999; Thornton et al. 2000). The
247 dataset is produced using an algorithmic technique that ingests point station measurements in
248 conjunction with a truncated Gaussian weighting filter. Some adjustments are made to account for
249 topography. Daymet is available through the Oak Ridge National Laboratory Distributed Active
250 Archive Center (ORNL DAAC).

251 *d. Methodology*

252 We have analyzed both the near surface (2 meter) temperature and precipitation over California,
253 in order to assess the models' performances in representing the mean climatology. Specifically,
254 evaluation will focus on daily maximum, minimum and average 2m temperatures (Tmax, Tmin
255 and Tavg), and daily precipitation (Pr). These variables are key for a baseline climate assessment,
256 particularly for their relationship with water resources, agriculture and health. With the overall
257 warm climate and large impact of heat waves over CA, we will focus on the summer season over
258 June, July and August (JJA) in the aspect of temperature. Since the vast majority of precipitation

259 in CA occurs in the winter season, together with the accumulation of snowpack, in this way,
260 precipitation over December-January-February (DJF) will be emphasized. Those seasons also
261 represent the most part of the climate variability.

262 In order to adequately account for natural variability even regionally, simulations need to be
263 run long enough (?). However, there is no particular timeframe for climatology studies. Aver-
264 age weather conditions over 30-year or so are typically used to track climate to make sure that
265 the data is long enough to calculate an average that is not influenced by year-to-year variability
266 (Dinse 2009). In this study, 26-year current-climate runtime is chosen to reasonably balance the
267 reproducibility and computational availability. We have studied the variability of mean tempera-
268 ture and precipitation in both simulations and observations over 5, 10, 20 and 25 seasons or years,
269 and the results showed that 20 or 25 years' simulation are long enough to adequately capture the
270 regionally climate variability. 30 years or longer run time may sound better, but are not necessary
271 for our case.

272 All the results showed in the following part are based on the time period year 1980 to 2005. All
273 the datasets have been investigated first to see if time trend exists over this 26 years period, and
274 the least squares linear trend has been removed from original datasets if existing. It is found that
275 for temperature, there do exist statistically significant linear trend over some parts of CA under the
276 two-tailed t-statistic significance level of 0.05. However, no significant trend has been detected for
277 precipitation.

278 Further, in order to better assess the treatment of California's varied climate regions, the state
279 has been divided into five regional zones, including: the Central Valley, Mountain Region, North
280 Coast, South Coast, and Desert Region (Figure 1). The division of these five zones are loosely
281 based on the results of Abatzoglou et als study (Abatzoglou et al. 2009) and the building climates
282 zones from California Energy Commission. For parts of the results analyses, simulations and

283 datasets are masked to restrict climate variables to specific zones. We aim to examine the statistics
284 of data averaged over geographic climate zones instead of just on grid-cell analysis.

285 Some statistical measurements have been used to quantify the performances of the models com-
286 paring with the reference datasets. These statistical variables include the Root-mean-square devia-
287 tion (RMSD), mean absolute difference (MAD), mean relative difference (MRD) and correlation,
288 and sample standard deviation.

289 When calculating the difference at grid point, the reference datasets are remapped to the given
290 model's output resolution. Datasets are remapped using a bilinear interpolation method, which
291 has been verified to provide satisfactory performance. Other remapping algorithms, such as patch-
292 based have been tested and do not exhibit notable differences.

293 Student's t-test is used when necessary to see if two sets of yearly or seasonally averaged data are
294 significantly different from each other, and 0.05 is used as critical levels of significance. We need
295 to point out that this is just a approximate test to further support our results analysis since the two
296 populations being compared should follow a normal distribution.

297 **3. Results**

298 *a. Temperature*

299 The mean JJA Tmax, Tmin and Tavg climatology over 26 years are shown in Figure 4. And the
300 statistical measurements over whole CA area are showed in Table 2. All simulations captured the
301 spatial climate patterns showed by the PRISM, with high spatial correlations (>0.95), especially
302 for Tmax and Tavg. For Tmax, comparing reference datasets, CESM simulations showed warmer
303 climate generally, especially uniform CESM. However, WRF output displayed overall colder cli-

304 mate, especially the WRF 9km. Tmax overall Central Valley has been overestimated by all the
305 simulations.

306 For Tmin, varres-CESM showed a larger warm effect, with a particularly egregious overestima-
307 tion of Tmin over Nevada (although difference are much smaller when focusing exclusively on
308 California). Comparing with reference datasets, WRF had better performance than varres-CESM
309 with smaller differences, especially for WRF 9km. However, the pattern of Tmin present in Figure
310 4 in both WRF simulations suggests a cooler interior to the Central Valley and warmer perimeter,
311 which is not supported by observations. Overestimation of Tmin by varres-CESM leads a similar
312 overestimation for Tavg. And underestimation of Tmax by WRF, causes a underestimation for
313 Tavg, but still statistically more close to reference datasets than CESMs. The sample standard de-
314 viation of the JJA Tmax, Tmin and Tavg by models and PRISM are showed in Figure 5. It can be
315 seen that the variability has little changes across difference sub-zones, and the values are around
316 0.5 to 1.5 °Cfor all the datasets, except some higher values over mountains regions in WRF 9km.

317 The RMSD values between the models and reference datasets range from 2 to 4°C. We have
318 made the Student's t-test to test the if the mean temperature climatology from PRISM, UW and
319 Daymet are statistically different from each other. And the results we got is that they are the same
320 at the significance level of 0.05 over most regions of our study area, except coastal regions. There
321 are some minor uncertainties, as we already discussed, showed when comparing with different
322 reference datasets. However, it can still be seen that varres-CESM is comparable to WRF and
323 uniform CESM, without meaning that they are statistically the same. Overall, varres-CESM 0.125
324 degree performed better in simulating long-term Tmax, WRF is better at modeling Tmin than
325 varres-CESM. Varres-CESM overestimated all JJA temperatures (especially Tmin), whereas WRF
326 underestimates Tmax and Tavg. When comparing against NARR (not showed), the overestimation
327 of Tmin are largely reduced for varres-CESM. This suggests that the source of the temperature

328 bias in varres-CESM and NARR may be related. Also, there are a positive 2 K SST bias near
329 the California coastline, when comparing varres-CESM and WRF simulations. This may cause
330 overestimation of temperatures.

331 This is especially encouraging since differences in the varres-CESM simulations, which only
332 used prescribed SSTs, closely matched those of WRF, which were also forced at the lateral domain
333 boundaries with reanalysis data. Differences between the reference datasets is relatively smaller
334 than between the models and reference datasets, thus uncertainties are unlikely impacting the
335 evaluation results. Also, the sea breeze effect, associated with cooler temperatures near the San
336 Francisco Bay, are apparent in all runs.

337 The seasonal cycle of Tavg is shown in Figure 7 for simulations and reference data from PRISM
338 and NARR. The models do show good consistency with reference data with no larger than a 2°C
339 difference, which mainly occurred in the coldest and hottest seasons. Compared with PRISM,
340 Varres-CESM showed positive difference over the summer season in all sub-zones except coastal
341 regions, and negative difference over winter season in all zones. The uniform CESM is similar to
342 varres-CESM, with larger difference. WRF showed better performance in presenting the monthly
343 trend than CESM with a little underestimation over all seasons. No notable differences can be
344 discerned when comparing models across resolutions.

345 The variability over each month is expressed by the sample standard deviation showed in Figure
346 ???. Generally, local variability of Tavg is under the magnitude of 3°C, mostly within the range
347 from 1 to 2°C. Among the simulations, WRF 27km is most consistent with PRISM. WRF 9km
348 is also close to PRISM, but has 1°C larger variability over January and February. Varres-CESM
349 basically showed about 0.5°C more scattered values (either above or lower) comparing to reference
350 datasets, and uniform CESM has a about 0.5°C lower variability than others.

351 For the temperature climatology in California, we are most interested in the Tmax over summer
352 season due to the impact of summer heat extremes. We depict the frequency distribution of Tmax
353 using all the JJA daily values over 26 years. The results of the simulations and reference datasets
354 including Daymet and UW are showed in Figure 8. Properties of the Frequency distribution, in-
355 cluding average, variability, skewness and Kurtosis are tabulated in Table ???. Though with some
356 deviations, similar distribution shapes with tails off to left are present for both models and obser-
357 vations. Contrasting with WRF, varres-CESMs are more close to reference datasets. WRF 9km
358 tended to be colder. Models including varres-CESM and WRF 27km are more consistent with
359 observations for higher values than the peak and less consistent at lower values. For representa-
360 tion of heat extremes, both varres-CESM and WRF 27km exhibit satisfactory performance over
361 most regions except in Central Valley (CV). No obvious improvement is associated with higher
362 resolution in varres-CESM.

363 In the CV, the models show a clear warm effect and associated long tail, with temperatures
364 reaching near 50°C. As discussed before, all models do overestimate Tmax in the CV. In order to
365 further assess the accuracy of the gridded observations, we examine the Tmax data directly from
366 recorded weather station observations over the CV. The results validate that Tmax values above
367 45°C are rare (although station observations suggest these days may be slightly more frequent
368 than suggested by UW and Daymet). The warm bias associated with the aforementioned extreme
369 hot days in both varres-CESM and WRF is likely due to reasons discussed in Caldwell et al.
370 (2009) where biases were correlated with overly dry summertime soil moisture. This could be
371 caused by the lack of accurate land surface treatment in climate models. areas. Bonfils and Lobell
372 (2007) found that irrigation in California's Central Valley has significantly decreased summertime
373 maximum temperatures especially in heavily-irrigated areas (Bonfils and Lobell 2007). Other

³⁷⁴ studies can also be found for the cooling climatic effects of irrigation, such as (Kueppers et al.
³⁷⁵ 2007).

³⁷⁶ *b. Precipitation*

³⁷⁷ California is known for the shortage of natural water resources with extreme drought over sum-
³⁷⁸ mer season. Instead, the winter season is particularly important for California as it accounts for 50
³⁷⁹ percent of the 22.5 inches that California receives for its total annual average precipitation amounts
³⁸⁰ (<http://www.ncdc.noaa.gov/cag/>).

³⁸¹ The long-term average climatologies of DJF and annual daily precipitation (Pr) over 26 years
³⁸² from simulations and reference datasets are displayed in Figure ???. And the statistical measure-
³⁸³ ments over whole CA area are showed in Table ???. As we can see, precipitation is distributed
³⁸⁴ mostly along the North coast and Sierra Nevada mountains, and is relatively sparse in other re-
³⁸⁵ gions. As temperature, simulations also captured the spatial patterns of the PRISM, with high
³⁸⁶ correlation coefficients (>0.94). However, there does exist clear differences among simulations.

³⁸⁷ Varres-CESM overestimates total precipitation, especially in the coarse resolution (28 km) sim-
³⁸⁸ ulation (about 40%-50%) along the western side of Sierra Nevada resulting statistical difference
³⁸⁹ over this area comparing with PRISM. The finer resolution simulation produces a slight reduction
³⁹⁰ of difference with magnitude near 1 mm/day, likely due to improved treatment of orographic ef-
³⁹¹ fects as showed in Figure 3. Interestingly, varres-CESM 0.125° is statistically the same as PRISM.
³⁹² Uniform CESM has slighter better results than varres-CESM 0.25deg. Notably, there are large dif-
³⁹³ ferences between WRF 27km and WRF 9km. WRF 27km underestimates precipitation slightly
³⁹⁴ (about 30%), whereas WRF 9km shows a large positive difference (about 70%-80%) along the
³⁹⁵ North coast and the Sierra Nevada of up to 50 percent. However, WRF 9km and WRF 27km are
³⁹⁶ both significantly the same at the significance level of 0.05 as PRISM except the mountain region,

397 considering the variability within them as showed in the Figure 10. From the sample standard
398 deviation of the precipitation displayed in Figure 10, we can see that the variability has similar
399 patterns of the precipitation intensity distribution, and increases as the precipitation magnitude
400 increases. Models seems capture the variation of precipitation well except the 50% higher values
401 of WRF 9km, and the varres-CESM 0.125deg and WRF 27 km showed more realistic values than
402 others comparing with PRISM.

403 The reference datasets also have notable differences indicating uncertainty inherent in interpo-
404 lating station data to a grid. However, these observations are still of the highest quality available
405 and the uncertainty is relatively small compared with difference from the simulations. We have
406 also made the Student's t-test to test the if the mean precipitation climatology from PRISM, UW
407 and Daymet are statistically different from each other. And the results we got is that they are al-
408 most the same at the significance level of 0.05 over all the study area. Therefore, the uncertainties
409 within them are negligible. Overall, varres-CESM 0.125° performs slightly better than CESM
410 0.25° and WRF 27km, as further exhibited by the RMSD values in Table 4.

411 The climatological annual cycle of precipitation averaged over each sub-region is presented in
412 Figure 12. It can be seen that simulations showed similar trend as reference datasets. The main
413 deviation occurred during the rainy seasons, especially in winter. WRF 27km is drier in all regions
414 and WRF 9km is far wetter in all regions. Varres-CESM tracks well with observed precipitation
415 everywhere except in the Central Valley, where precipitation is overestimated. Nonetheless, the
416 strong seasonal dependence on precipitation is apparent in all regions with extremely dry condi-
417 tions during summer months. A slight increase in summertime precipitation is apparent in the
418 Desert region, indicating the North American monsoon. Overall, varres-CESM is more consis-
419 tent with observations in most regions and in all seasons compared with WRF. However, we also
420 observe that the peak month for precipitation tends to occur earlier in varres-CESM than in obser-

vations. It is not surprising that a seasonal time drift occurred with the varres-CESM simulations as it was not forced by a reanalysis dataset (unlike the WRF simulations).

The variability over each month is expressed by the sample standard deviation showed in Figure ???. It can be seen that variability has similar monthly trend as the annual cycle of precipitation, with overall value from 0 to 4 mm/day, which generally shows higher interannual variability over locations of higher mean precipitation 12. Varres-CESM also exhibited a slightly larger variability in the rainy season than observations, while WRF 27km showed a little reduced values. WRF 9km showed notable larger variability compared with observations during rainy seasons over most regions. Such higher variability within finer resolution has also been found in previous studies. Duffy et al. (2006) discussed the higher variability caused by higher spatial resolution used in RCM models, allowing more accurate representation of topography, which is likely, at least in part, to be the reason (?). The main cause of the interannual variability of precipitation over CA is El NioSouthern Oscillation (ENSO), which varies the amount of moisture flux transported to this region.

The frequency distribution of DJF Pr has been constructed from rainy days in winter ($\text{Pr} \geq 0.1 \text{mm/d}$) and depicted in Figure 13. It can be seen that varres-CESM is more consistent with observations everywhere except in the CV. In this region WRF 27km appears to better capture high-intensity precipitation events, but performs more poorly on low-intensity events. The underestimation of rainfall frequency in WRF 27km appears consistent across regions. WRF 9km produces a significantly better treatment of low-intensity events, but greatly overestimates the frequency of high-intensity events. Notably, varres-CESM 0.25 degree and varres-CESM 0.125 degree do not show significant differences. For strong precipitation events, varres-CESM and WRF 27km show good performance over most regions except in those noted above, although these conclusions are also constrained by observational uncertainty.

445 The positive deviation of precipitation using WRF at high resolution has also been found in
446 former studies. Caldwell et al. (2009) also showed that WRF at 12km largely overestimate the
447 precipitation over the mountain division of CA. The deviation magnitude is less than what showed
448 in this study due to different division area and different setting of microphysics. In Caldwell's
449 paper aforementioned, possible reasons have been discussed in detail, stating a variety of source
450 including the model itself and the choice of physical parameterizations. A comprehensive analysis
451 of the cause of these errors is beyond the scope of this paper. Further discussion can be found in
452 former studies including the use of different microphysics schemes and resulting change of pre-
453 cipitation magnitude (?Jankov et al. 2005; Gallus Jr and Bresch 2006; Chin et al. 2010; Caldwell
454 2010).

455 Finally, a concise summary of model performance over CA is provided by the Taylor diagram
456 (Figure 14). This diagram includes the spatial centered correlation between the simulated and
457 observed fields, the RMS variability of simulations normalized by that in the observations, and
458 mean differences from reference data. It can be seen that the models correlate well with the PRISM
459 reference dataset. Normalized standard deviation and bias are larger for precipitation, especially
460 for WRF 9km. Overall, varres-CESM has demonstrated that it can competitively compare to WRF
461 in capturing the regional climatology of California. ([update the plot](#))

462 **4. Discussions and summary**

463 This study has evaluated the performance of a relatively new variable-resolution GCM model,
464 i.e. varres-CESM in simulating California climatology for regional climate studies. This new tech-
465 nique is studied against WRF as a traditional RCM. Gridded datasets are used to help us evaluate
466 the modeling results. As the need for assessments of regional climate change is increasing, alter-
467 native modeling strategies, including variable-resolution global climate models will be needed to

⁴⁶⁸ improve our understanding of the effects of fine-scale processes representation in regional climate
⁴⁶⁹ regulation.

⁴⁷⁰ Based on 26 years of high-resolution historical climate simulations, we analyzed both tempera-
⁴⁷¹ ture and precipitation in California and across its climate divisions. We found that varres-CESM
⁴⁷² output have comparable performance as WRF for mean climatology, although the model still pos-
⁴⁷³ sessed a slight tendency to a warmer and moister climate, especially in the Central Valley which
⁴⁷⁴ is surrounded by mountain and coastal region. WRF exhibited a clear colder summer Tmax over
⁴⁷⁵ most regions except the Central Valley, but a little warmer in summer Tmin. Varres-CESM showed
⁴⁷⁶ better ability in reproducing Tmax, however, looking at the magnitude of statistical measurements,
⁴⁷⁷ WRF was better at modeling Tmin and Tavg. WRF presents the monthly trend better than CESM
⁴⁷⁸ with a little underestimation over all seasons, with smaller temperature range.

⁴⁷⁹ For representation of heat extremes, both varres-CESM and WRF 27km exhibit satisfactory
⁴⁸⁰ performance over most regions except in Central Valley (CV). This is likely caused by the loss
⁴⁸¹ of irrigation cooling effect over this region and irrigation effect is rarely considered in long-term
⁴⁸² climate modeling. In future work, we will add irrigation effect in varres-CESM to figure out the
⁴⁸³ role irrigation played in regulating Tmax, to reduce the overestimation and longer upbounded tail
⁴⁸⁴ of frequency distribution for Tmax,

⁴⁸⁵ The main precipitation modeling deviations occurred during rainy seasons, especially in win-
⁴⁸⁶ ter. Varres-CESM overestimates precipitation especially along the western side of Sierra Nevada,
⁴⁸⁷ though the finer resolution simulation produces a slight reduction likely due to improved treatment
⁴⁸⁸ of orographic effects. WRF 27km underestimates precipitation slightly, whereas WRF 9km shows
⁴⁸⁹ a large overestimation. It can be seen that simulations showed similar seasonal trend as refer-
⁴⁹⁰ ence datasets, with main deviation occurred during the rainy seasons. Varres-CESM also exhibited
⁴⁹¹ a slightly larger variability than WRF 27km. For strong precipitation events, varres-CESM and

492 WRF 27km show satisfactory modeling ability over most regions (except the Central Valley, in the
493 case of varres-CESM), although the reference datasets also show some uncertainties.

494 Higher resolution (0.125°) simulations with varres-CESM were quite similar to the coarser reso-
495 lution runs, although there were not too significant improvements in capturing summer Tmax and
496 precipitation, and their corresponding variability. For WRF, simulation at finer resolution (9km)
497 also did not really show meaningful improvement in representing finer regional climatology. When
498 resolution increased, WRF produce a obviously overestimated precipitation over the North coastal
499 region and the mountain region. This is not surprising since previous studies have also found
500 this phenomenon for fine-scale simulations using RCMs as aforementioned. The use convection
501 scheme is perhaps not needed when grid spacing is near 10km. However, it turned out that almost
502 all of the precipitation comes from resolved (large-scale) processes for all these models. In this
503 way, model deviation is mainly related with resolved-scale processes and microphysics scheme
504 plays a major role, which makes it necessary to develop more scale-aware parameterizations.

505 The importance and necessity of high resolution for regional climate studies has been widely
506 stressed by previous studies. However, whether the current regional climate models can fulfill this
507 demand when resolution is pushed to local scales is questionable. It is clear that further work is
508 urgently needed to solve the scale limitation of current regional climate models at fine horizontal
509 resolutions. The possible causes of the scale limitation may include a lack of accurate scale-aware
510 physical parameterizations near or below 10 km horizontal resolution, the treatment of dynamics
511 at fine scales, and the interactions among different components of RCMs or VR-GCMs (e.g., land-
512 atmosphere interactions).

513 Generally, when compared with reference datasets, simulations do a good job of capturing re-
514 gional climatological patterns with high spatial correlations. Deviations are not indicative of deep
515 underlying problems with the model formulation, but one should be aware of these differences

516 when using these models for assessing future climate change. Uncertainty between observational
517 datasets exists, but is relatively small. Compared with the uniform resolution CESM-FV sim-
518 ulation, varres-CESM performed similarly or even a little better in some cases, which gives us
519 more confidence to use this technique in further climate change studies. In summary, varres-
520 CESM demonstrated competitive utility for studying high-resolution regional climatology when
521 compared to a regional climate model (WRF) and a uniform high-resolution GCM (CESM-FV).
522 This study suggests that variable-resolution GCMs are useful tools for assessing climate change
523 over the coming century.

524 *Acknowledgments.* The authors would like to thank Michael Wehner and Daíthí Stone for pro-
525 viding the uniform resolution CESM dataset. We would further like to thank Travis O'Brien for
526 his many useful conversations on climate model assessment. We also want to thank Xuemeng
527 Chen for her assistance in WRF running. This project is supported in part by the University of
528 California, Davis and by the Department of Energy “Multiscale Methods for Accurate, Efficient,
529 and Scale-Aware Models of the Earth System” program.

530 References

- 531 Abatzoglou, J. T., K. T. Redmond, and L. M. Edwards, 2009: Classification of regional climate
532 variability in the state of California. *Journal of Applied Meteorology and Climatology*, **48** (8),
533 1527–1541.
- 534 Bacmeister, J. T., M. F. Wehner, R. B. Neale, A. Gettelman, C. Hannay, P. H. Lauritzen, J. M.
535 Caron, and J. E. Truesdale, 2014: Exploratory high-resolution climate simulations using the
536 Community Atmosphere Model (CAM). *Journal of Climate*, **27** (9), 3073–3099.

- 537 Bonfils, C., and D. Lobell, 2007: Empirical evidence for a recent slowdown in irrigation-induced
538 cooling. *Proceedings of the National Academy of Sciences*, **104** (34), 13 582–13 587.
- 539 Bukovsky, M. S., and D. J. Karoly, 2007: A brief evaluation of precipitation from the North
540 American Regional Reanalysis. *Journal of Hydrometeorology*, **8** (4), 837–846.
- 541 Bukovsky, M. S., and D. J. Karoly, 2009: Precipitation simulations using WRF as a nested regional
542 climate model. *Journal of Applied Meteorology and Climatology*, **48** (10), 2152–2159.
- 543 Caldwell, P., 2010: California wintertime precipitation bias in regional and global climate models.
544 *Journal of Applied Meteorology and Climatology*, **49** (10), 2147–2158.
- 545 Caldwell, P., H.-N. S. Chin, D. C. Bader, and G. Bala, 2009: Evaluation of a WRF dynamical
546 downscaling simulation over California. *Climatic Change*, **95** (3-4), 499–521.
- 547 Cayan, D. R., A. L. Luers, G. Franco, M. Hanemann, B. Croes, and E. Vine, 2008: Overview of
548 the California climate change scenarios project. *Climatic Change*, **87** (1), 1–6.
- 549 Chen, F., and J. Dudhia, 2001: Coupling an advanced land surface-hydrology model with the Penn
550 State-NCAR MM5 modeling system. Part I: Model implementation and sensitivity. *Monthly
551 Weather Review*, **129** (4), 569–585.
- 552 Chin, H.-N. S., P. M. Caldwell, and D. C. Bader, 2010: Preliminary study of California wintertime
553 model wet bias. *Monthly Weather Review*, **138** (9), 3556–3571.
- 554 Christensen, J. H., and Coauthors, 2007: Regional climate projections. *Climate Change, 2007:*
555 *The Physical Science Basis. Contribution of Working group I to the Fourth Assessment Report
556 of the Intergovernmental Panel on Climate Change, University Press, Cambridge, Chapter 11,*
557 847–940.

- 558 Collins, W. D., and Coauthors, 2004: Description of the NCAR community atmosphere model
559 (CAM 3.0). Tech. rep., Tech. Rep. NCAR/TN-464+ STR.
- 560 Daly, C., M. Halbleib, J. I. Smith, W. P. Gibson, M. K. Doggett, G. H. Taylor, J. Curtis, and P. P.
561 Pasteris, 2008: Physiographically sensitive mapping of climatological temperature and precip-
562 itation across the conterminous United States. *International Journal of Climatology*, **28** (15),
563 2031–2064.
- 564 Dee, D., and Coauthors, 2011: The ERA-Interim reanalysis: Configuration and performance of
565 the data assimilation system. *Quarterly Journal of the Royal Meteorological Society*, **137** (656),
566 553–597.
- 567 Dinse, K., 2009: Climate variability and climate change: what is the difference. *Book Climate
568 Variability and Climate Change: What is the Difference*.
- 569 Fowler, H., S. Blenkinsop, and C. Tebaldi, 2007: Linking climate change modelling to impacts
570 studies: recent advances in downscaling techniques for hydrological modelling. *International
571 Journal of Climatology*, **27** (12), 1547–1578.
- 572 Fox-Rabinovitz, M., J. Côté, B. Dugas, M. Déqué, and J. L. McGregor, 2006: Variable resolution
573 general circulation models: Stretched-grid model intercomparison project (SGMIP). *Journal of
574 Geophysical Research: Atmospheres (1984–2012)*, **111** (D16).
- 575 Fox-Rabinovitz, M. S., G. L. Stenchikov, M. J. Suarez, and L. L. Takacs, 1997: A finite-
576 difference GCM dynamical core with a variable-resolution stretched grid. *Monthly Weather
577 Review*, **125** (11), 2943–2968.

- 578 Fox-Rabinovitz, M. S., L. L. Takacs, R. C. Govindaraju, and M. J. Suarez, 2001: A variable-
579 resolution stretched-grid general circulation model: Regional climate simulation. *Monthly*
580 *Weather Review*, **129** (3), 453–469.
- 581 Gallus Jr, W. A., and J. F. Bresch, 2006: Comparison of impacts of WRF dynamic core, physics
582 package, and initial conditions on warm season rainfall forecasts. *Monthly Weather Review*,
583 **134** (9), 2632–2641.
- 584 Gates, W. L., 1992: AMIP: The Atmospheric Model Intercomparison Project. *Bulletin of the*
585 *American Meteorological Society*, **73**, 1962–1970.
- 586 Hamlet, A. F., and D. P. Lettenmaier, 2005: Production of Temporally Consistent Gridded Precipi-
587 tation and Temperature Fields for the Continental United States*. *Journal of Hydrometeorology*,
588 **6** (3), 330–336.
- 589 Hayhoe, K., and Coauthors, 2004: Emissions pathways, climate change, and impacts on Califor-
590 nia. *Proceedings of the National Academy of Sciences of the United States of America*, **101** (34),
591 12 422–12 427.
- 592 Hong, S.-Y., and J.-O. J. Lim, 2006: The WRF single-moment 6-class microphysics scheme
593 (WSM6). *Asia-Pacific Journal of Atmospheric Sciences*, **42** (2), 129–151.
- 594 Hong, S.-Y., Y. Noh, and J. Dudhia, 2006: A new vertical diffusion package with an explicit
595 treatment of entrainment processes. *Monthly Weather Review*, **134** (9), 2318–2341.
- 596 Hurrell, J. W., J. J. Hack, D. Shea, J. M. Caron, and J. Rosinski, 2008: A new sea surface temper-
597 ature and sea ice boundary dataset for the Community Atmosphere Model. *Journal of Climate*,
598 **21** (19), 5145–5153.

- 599 Hurrell, J. W., and Coauthors, 2013: The community earth system model: A framework for col-
600 laborative research. *Bulletin of the American Meteorological Society*, **94** (9), 1339–1360.
- 601 Jankov, I., W. A. Gallus Jr, M. Segal, B. Shaw, and S. E. Koch, 2005: The impact of different WRF
602 model physical parameterizations and their interactions on warm season MCS rainfall. *Weather*
603 and Forecasting, **20** (6), 1048–1060.
- 604 Kain, J. S., 2004: The Kain-Fritsch convective parameterization: An update. *Journal of Applied*
605 *Meteorology*, **43** (1), 170–181.
- 606 Kanamitsu, M., and H. Kanamaru, 2007: Fifty-seven-year California Reanalysis Downscaling at
607 10 km (CaRD10). Part I: System detail and validation with observations. *Journal of Climate*,
608 **20** (22), 5553–5571.
- 609 Kueppers, L. M., M. A. Snyder, and L. C. Sloan, 2007: Irrigation cooling effect: Regional climate
610 forcing by land-use change. *Geophysical Research Letters*, **34** (3).
- 611 Laprise, R., 2008: Regional climate modelling. *Journal of Computational Physics*, **227** (7), 3641–
612 3666.
- 613 Laprise, R., and Coauthors, 2008: Challenging some tenets of regional climate modelling. *Meteo-*
614 *rology and Atmospheric Physics*, **100** (1-4), 3–22.
- 615 Leung, L. R., L. O. Mearns, F. Giorgi, and R. L. Wilby, 2003: Regional climate research: needs
616 and opportunities. *Bulletin of the American Meteorological Society*, **84** (1), 89–95.
- 617 Leung, L. R., and Y. Qian, 2009: Atmospheric rivers induced heavy precipitation and flooding in
618 the western US simulated by the WRF regional climate model. *Geophysical research letters*,
619 **36** (3).

- 620 Leung, L. R., Y. Qian, X. Bian, W. M. Washington, J. Han, and J. O. Roads, 2004: Mid-century
621 ensemble regional climate change scenarios for the western United States. *Climatic Change*,
622 **62 (1-3)**, 75–113.
- 623 Lo, J. C.-F., Z.-L. Yang, and R. A. Pielke, 2008: Assessment of three dynamical climate downscal-
624 ing methods using the Weather Research and Forecasting (WRF) model. *Journal of Geophysical*
625 *Research: Atmospheres (1984–2012)*, **113 (D9)**.
- 626 Maurer, E., A. Wood, J. Adam, D. Lettenmaier, and B. Nijssen, 2002: A long-term hydrologically
627 based dataset of land surface fluxes and states for the conterminous United States*. *Journal of*
628 *climate*, **15 (22)**, 3237–3251.
- 629 McDonald, A., 2003: Transparent boundary conditions for the shallow-water equations: testing in
630 a nested environment. *Monthly Weather Review*, **131 (4)**, 698–705.
- 631 Mearns, L. O., and Coauthors, 2012: The North American regional climate change assessment
632 program: overview of phase I results. *Bulletin of the American Meteorological Society*, **93 (9)**,
633 1337–1362.
- 634 Mesinger, F., and K. Veljovic, 2013: Limited area NWP and regional climate modeling: a test
635 of the relaxation vs Eta lateral boundary conditions. *Meteorology and Atmospheric Physics*,
636 **119 (1-2)**, 1–16.
- 637 Mesinger, F., and Coauthors, 2006: North American regional reanalysis. *Bulletin of the American*
638 *Meteorological Society*, **87**, 343–360.
- 639 Neale, R. B., and Coauthors, 2010a: Description of the NCAR community atmosphere model
640 (CAM 5.0). *NCAR Tech. Note NCAR/TN-486+ STR*.

- 641 Neale, R. B., and Coauthors, 2010b: Description of the NCAR Community Atmosphere Model
642 (CAM 5.0). NCAR Technical Note NCAR/TN-486+STR, National Center for Atmospheric Re-
643 search, Boulder, Colorado, 268 pp.
- 644 Oleson, K., and Coauthors, 2010: Technical description of version 4.0 of the Community Land
645 Model (CLM). NCAR Technical Note NCAR/TN-478+STR, National Center for Atmospheric
646 Research, Boulder, Colorado, 257 pp. doi:10.5065/D6FB50WZ.
- 647 Pan, L.-L., S.-H. Chen, D. Cayan, M.-Y. Lin, Q. Hart, M.-H. Zhang, Y. Liu, and J. Wang, 2011:
648 Influences of climate change on California and Nevada regions revealed by a high-resolution
649 dynamical downscaling study. *Climate Dynamics*, **37 (9-10)**, 2005–2020.
- 650 Pierce, D. W., and Coauthors, 2013: Probabilistic estimates of future changes in California temper-
651 ature and precipitation using statistical and dynamical downscaling. *Climate Dynamics*, **40 (3-**
652 **4)**, 839–856.
- 653 Rauscher, S. A., E. Coppola, C. Piani, and F. Giorgi, 2010: Resolution effects on regional climate
654 model simulations of seasonal precipitation over Europe. *Climate Dynamics*, **35 (4)**, 685–711.
- 655 Rauscher, S. A., T. D. Ringler, W. C. Skamarock, and A. A. Mirin, 2013: Exploring a Global
656 Multiresolution Modeling Approach Using Aquaplanet Simulations. *Journal of Climate*, **26 (8)**,
657 2432–2452.
- 658 Skamarock, W., J. Klemp, J. Dudhia, D. Gill, and D. Barker, 2005: Coauthors, 2008: A Descrip-
659 tion of the Advanced Research WRF Version 3. NCAR Technical Note. Tech. rep., NCAR/TN–
660 475+ STR.

- 661 Skamarock, W. C., and J. B. Klemp, 2008: A time-split nonhydrostatic atmospheric model for
662 weather research and forecasting applications. *Journal of Computational Physics*, **227** (7),
663 3465–3485.
- 664 Soares, P. M., R. M. Cardoso, P. M. Miranda, J. de Medeiros, M. Belo-Pereira, and F. Espírito-
665 Santo, 2012: WRF high resolution dynamical downscaling of ERA-Interim for Portugal. *Cli-
666 mate dynamics*, **39** (9-10), 2497–2522.
- 667 Staniforth, A. N., and H. L. Mitchell, 1978: A variable-resolution finite-element technique for
668 regional forecasting with the primitive equations. *Monthly Weather Review*, **106** (4), 439–447.
- 669 Stauffer, D. R., and N. L. Seaman, 1990: Use of four-dimensional data assimilation in a limited-
670 area mesoscale model. Part I: Experiments with synoptic-scale data. *Monthly Weather Review*,
671 **118** (6), 1250–1277.
- 672 Taylor, M. A., and A. Fournier, 2010: A compatible and conservative spectral element method on
673 unstructured grids. *Journal of Computational Physics*, **229** (17), 5879–5895.
- 674 Thornton, P. E., H. Hasenauer, and M. A. White, 2000: Simultaneous estimation of daily solar ra-
675 diation and humidity from observed temperature and precipitation: an application over complex
676 terrain in Austria. *Agricultural and Forest Meteorology*, **104** (4), 255–271.
- 677 Thornton, P. E., and S. W. Running, 1999: An improved algorithm for estimating incident daily
678 solar radiation from measurements of temperature, humidity, and precipitation. *Agricultural and
679 Forest Meteorology*, **93** (4), 211–228.
- 680 Thornton, P. E., S. W. Running, and M. A. White, 1997: Generating surfaces of daily meteorolog-
681 ical variables over large regions of complex terrain. *Journal of Hydrology*, **190** (3), 214–251.

- 682 Ullrich, P. A., 2014: SQuadGen: Spherical Quadrilateral Grid Generator. Accessed: 2015-02-11,
683 <http://climate.ucdavis.edu/squadgen.php>.
- 684 Warner, T. T., R. A. Peterson, and R. E. Treadon, 1997: A tutorial on lateral boundary conditions
685 as a basic and potentially serious limitation to regional numerical weather prediction. *Bulletin*
686 *of the American Meteorological Society*, **78** (11), 2599–2617.
- 687 Wehner, M., Prabhat, K. Reed, D. Stone, W. D. Collins, J. Bacmeister, and A. Gettleman, 2014a:
688 Resolution dependence of future tropical cyclone projections of CAM5.1 in the US CLIVAR
689 Hurricane Working Group idealized configurations. *J. Climate*, doi:10.1175/JCLI-D-14-00311.
690 1, in press.
- 691 Wehner, M. F., and Coauthors, 2014b: The effect of horizontal resolution on simulation qual-
692 ity in the Community Atmospheric Model, CAM5.1. *J. Model. Earth. Sys.*, doi:10.1002/
693 2013MS000276.
- 694 Zarzycki, C. M., and C. Jablonowski, 2014: A multidecadal simulation of Atlantic tropical cy-
695 clones using a variable-resolution global atmospheric general circulation model. *Journal of Ad-*
696 *vances in Modeling Earth Systems*, **6** (3), 805–828.
- 697 Zarzycki, C. M., C. Jablonowski, and M. A. Taylor, 2014: Using Variable-Resolution Meshes
698 to Model Tropical Cyclones in the Community Atmosphere Model. *Monthly Weather Review*,
699 **142** (3), 1221–1239.
- 700 Zarzycki, C. M., C. Jablonowski, D. R. Thatcher, and M. A. Taylor, 2015: Effects of localized
701 grid refinement on the general circulation and climatology in the community atmosphere model.
702 *Journal of Climate*, **28** (7), 2777–2803.

703 **LIST OF TABLES**

704 Table 1.	Reanalysis and statistically downscaled observational datasets used in this	34
705 study.		
706 Table 2.	RMSD, MAD and Correlation (Corr) for JJA temperature over California	35
707 Table 3.	The first four moments of the JJA Tmax frequency in each sub-zone. Column	
708 titles refer to Average (Avg), Variance (Var), Skewness (Skew) and Kurtosis		
709 (Kurt).		36
710 Table 4.	RMSD, MAD, MRD, Correlation (Corr) for precipitation over California	37

TABLE 1. Reanalysis and statistically downscaled observational datasets used in this study.

Data source	Variables used	Spatial resolution	Temporal resolution
NARR	Pr, T_s	32km	daily, 3-hourly
NCEP CPC	Pr	0.125°	daily
UW	Pr, T_{min} , T_{max}	0.125°	daily
PRISM	Pr, T_{min} , T_{max} , T_{avg}	4km	monthly
Daymet	Pr, T_{min} , T_{max}	1km	daily

TABLE 2. RMSD, MAD and Correlation (Corr) for JJA temperature over California

RMSD	UW		PRISM			Daymet	
	T_{max}	T_{min}	T_{max}	T_{min}	T_{avg}	T_{max}	T_{min}
varres-CESM 0.25d	2.322	3.745	2.924	3.121	2.604	2.810	3.934
varres-CESM 0.125d	1.900	3.631	2.447	2.944	2.184	2.475	3.701
WRF 27km	2.310	2.738	2.933	2.254	2.169	2.511	2.992
WRF 9km	3.319	2.937	3.492	1.837	1.769	3.203	2.942
uniform CESM 0.25d	3.885	4.088	4.265	3.614	3.536	4.315	4.274

MAD	UW		PRISM			Daymet	
	T_{max}	T_{min}	T_{max}	T_{min}	T_{avg}	T_{max}	T_{min}
varres-CESM 0.25d	0.981	2.907	0.606	1.731	0.823	1.177	2.877
varres-CESM 0.125d	0.645	2.848	0.203	1.660	0.579	0.818	2.744
WRF 27km	-0.577	0.819	-0.952	-0.357	-0.771	-0.386	0.789
WRF 9km	-2.277	1.862	-2.720	0.674	-1.142	-2.103	1.757
uniform CESM 0.25d	1.812	2.993	1.449	1.815	1.280	2.013	2.961

Corr	UW		PRISM			Daymet	
	T_{max}	T_{min}	T_{max}	T_{min}	T_{avg}	T_{max}	T_{min}
varres-CESM 0.25d	0.998	0.982	0.996	0.986	0.994	0.997	0.979
varres-CESM 0.125d	0.998	0.985	0.997	0.988	0.996	0.997	0.983
WRF 27km	0.997	0.982	0.996	0.989	0.996	0.997	0.978
WRF 9km	0.996	0.985	0.997	0.993	0.998	0.996	0.984
uniform CESM 0.25d	0.994	0.980	0.992	0.981	0.991	0.993	0.977

711 TABLE 3. The first four moments of the JJA Tmax frequency in each sub-zone. Column titles refer to Average
 712 (Avg), Variance (Var), Skewness (Skew) and Kurtosis (Kurt).

	Central valley				Mountain				North coast				South coast				Desert			
	Avg	Var	Skew	Kurt	Avg	Var	Skew	Kurt	Avg	Var	Skew	Kurt	Avg	Var	Skew	Kurt	Avg	Var	Skew	Kurt
UW	32.6	24.8	-0.8	0.9	26.7	33.2	-0.4	0.3	25.9	30.4	0.1	-0.5	25.9	30.4	0.1	-0.5	37.0	22.9	-0.6	0.7
Daymet	32.7	23.5	-0.9	1.5	25.9	39.3	-0.5	0.5	26.5	30.1	-0.3	0.4	26.5	30.1	-0.3	0.4	37.0	24.3	-0.6	0.6
CESM 0.25d	34.1	26.2	-0.4	0.2	28.1	27.6	-0.4	0.3	26.4	37.4	0.1	-0.7	26.4	37.4	0.1	-0.7	37.6	19.0	-0.5	0.8
CESM 0.125d	34.3	28.5	-0.5	0.4	27.2	30.0	-0.4	0.3	26.3	37.4	0.1	-0.6	26.3	37.4	0.1	-0.6	37.3	21.3	-0.5	0.4
WRF 27km	33.9	34.8	-0.5	0.2	24.9	34.8	-0.3	0.0	26.0	36.7	-0.1	-0.5	26.0	36.7	-0.1	-0.5	36.5	22.6	-0.6	0.5
WRF 9km	32.4	33.1	-0.7	0.6	22.4	38.5	-0.5	0.6	24.9	32.6	0.0	-0.6	24.9	32.6	0.0	-0.6	34.4	24.4	-0.5	0.4

Notes: If skew > 0 [skew < 0], the distribution trails off to the right [left]. If kurtosis > 0 [< 0], it is usually more sharply peaked [flatter] than the normal distribution (leptokurtic and platykurtic, respectively).

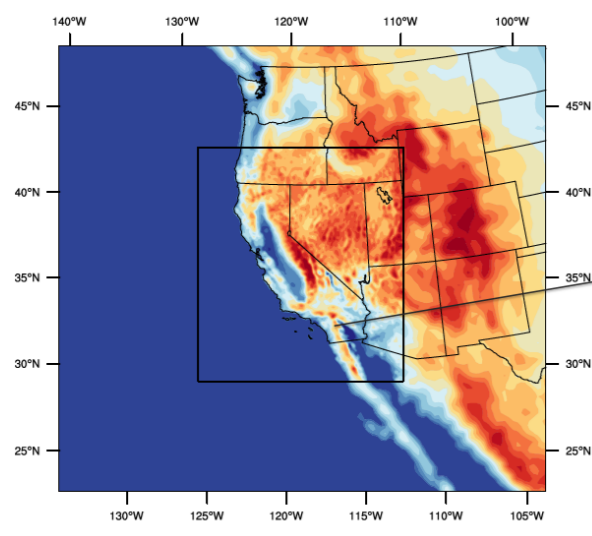
TABLE 4. RMSD, MAD, MRD, Correlation (Corr) for precipitation over California

Annual	CPC				UW				PRISM				DAYMET				
	RMSD	MAD	MRD	Corr	RMSD	MAD	MRD	Corr	RMSD	MAD	MRD	Corr	RMSD	MAD	MRD	Corr	
varres-CESM 0.25d	0.607	0.394	0.413	0.981	0.616	0.292	0.434	0.968	0.727	0.203	0.429	0.952	0.567	0.191	0.375	0.972	
varres-CESM 0.125d	0.469	0.207	0.321	0.980	0.526	0.115	0.339	0.970	0.624	0.045	0.328	0.961	0.504	0.027	0.310	0.973	
WRF 27km	0.419	-0.205	0.269	0.977	0.580	-0.308	0.274	0.971	0.765	-0.396	0.296	0.965	0.647	-0.409	0.312	0.970	
WRF 9km	2.226	1.485	0.950	0.957	2.052	1.393	0.864	0.964	1.889	1.322	0.815	0.970	2.005	1.306	0.773	0.961	
uniform CESM 0.25d	0.555	0.134	0.277	0.969	0.600	0.031	0.302	0.961	0.700	-0.057	0.290	0.953	0.600	-0.069	0.284	0.962	
DJF		CPC				UW				PRISM				DAYMET			
		RMSD	MAD	MRD	Corr	RMSD	MAD	MRD	Corr	RMSD	MAD	MRD	Corr	RMSD	MAD	MRD	Corr
varres-CESM 0.25d	1.486	0.986	0.532	0.972	1.445	0.673	0.531	0.959	1.654	0.577	0.547	0.943	1.346	0.514	0.435	0.964	
varres-CESM 0.125d	1.194	0.638	0.396	0.976	1.234	0.346	0.398	0.965	1.395	0.287	0.400	0.955	1.170	0.212	0.337	0.969	
WRF 27km	0.888	-0.376	0.269	0.975	1.289	-0.688	0.289	0.967	1.552	-0.785	0.298	0.962	1.351	-0.848	0.324	0.966	
WRF 9km	4.264	2.607	0.742	0.950	3.835	2.315	0.616	0.955	3.570	2.256	0.604	0.964	3.804	2.183	0.554	0.955	
uniform CESM 0.25d	1.392	0.377	0.300	0.960	1.431	0.064	0.316	0.951	1.544	-0.033	0.314	0.946	1.406	-0.095	0.288	0.953	

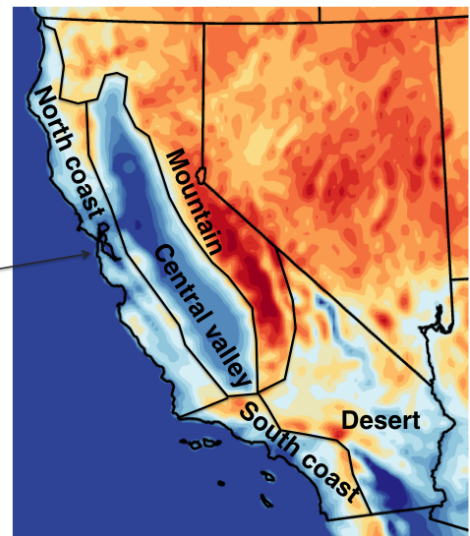
713 LIST OF FIGURES

714	Fig. 1. Domains of WRF simulations (left) and five climate divisions in California (right) with topography in meters (m).	39
715		
716	Fig. 2. Grid meshes for the two varres-CESM simulations.	40
717		
718	Fig. 3. Topography in meters (m) for (top left to bottom right) varres-CESM 0.25° , varres-CESM 0.125° , uniform CESM-FV 0.25° , WRF 27km, WRF 9km and ERA-Interim (~ 80 km).	41
719		
720	Fig. 4. JJA average daily Tmax, Tmin and Tavg from models and reference datasets, and differences between them ($^\circ\text{C}$).	42
721		
722	Fig. 5. sample standard deviation of JJA average daily Tmax, Tmin and Tavg from models and PRISM ($^\circ\text{C}$).	43
723		
724	Fig. 6. Seasonal cycle of monthly-average Tavg for each subzone ($^\circ\text{C}$). Bars represent standard deviation (σ) values.	44
725		
726	Fig. 7. Seasonal standard deviation (s) values of monthly-average Tavg for each subzone ($^\circ\text{C}$). Bars represent standard deviation (s) values.	45
727		
728	Fig. 8. Frequency distribution of summer Tmax ($^\circ\text{C}$).	46
729		
730	Fig. 9. Annual and DJF precipitation from models and reference datasets (mm/d).	47
731		
732	Fig. 10. sample standard deviation of Annual and DJF precipitation from models and PRISM (mm/d).	48
733		
734	Fig. 11. As Figure 6, but for monthly-average total precipitation (mm/d).	49
735		
736	Fig. 12. As Figure 7, but for monthly-average total precipitation (mm/d).	50
737		
738	Fig. 13. Frequency distribution of winter Pr constructed from 26 years of daily data (mm/d) (note that the vertical scale is logarithmic).	51
739		
740	Fig. 14. Taylor diagram of annual climatology for the entire California region, using the PRISM dataset as reference.	52

WRF 9km : Outer and inner domain

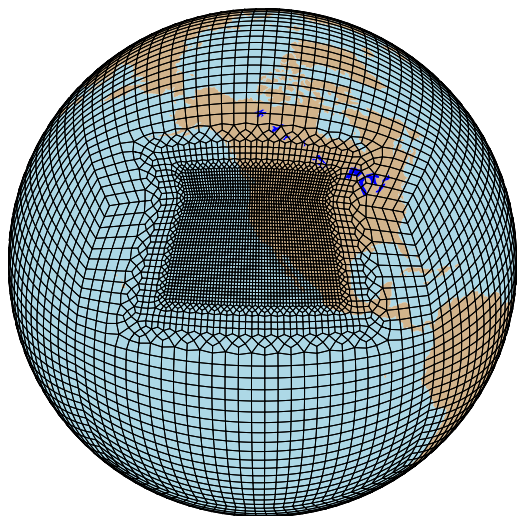


Climate divisions across CA



737 FIG. 1. Domains of WRF simulations (left) and five climate divisions in California (right) with topography in
738 meters (m).

1 degree -> 0.25 degree



1 degree -> 0.125 degree

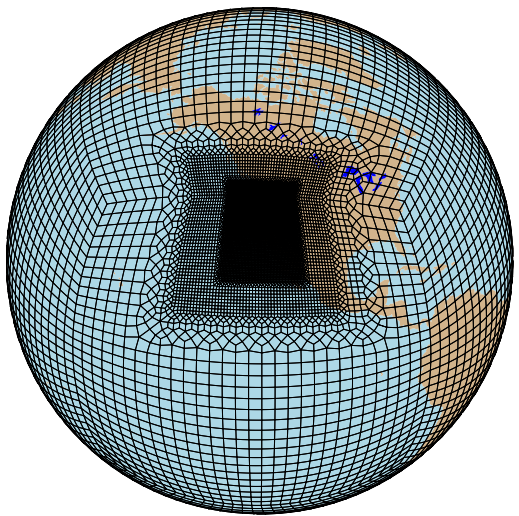
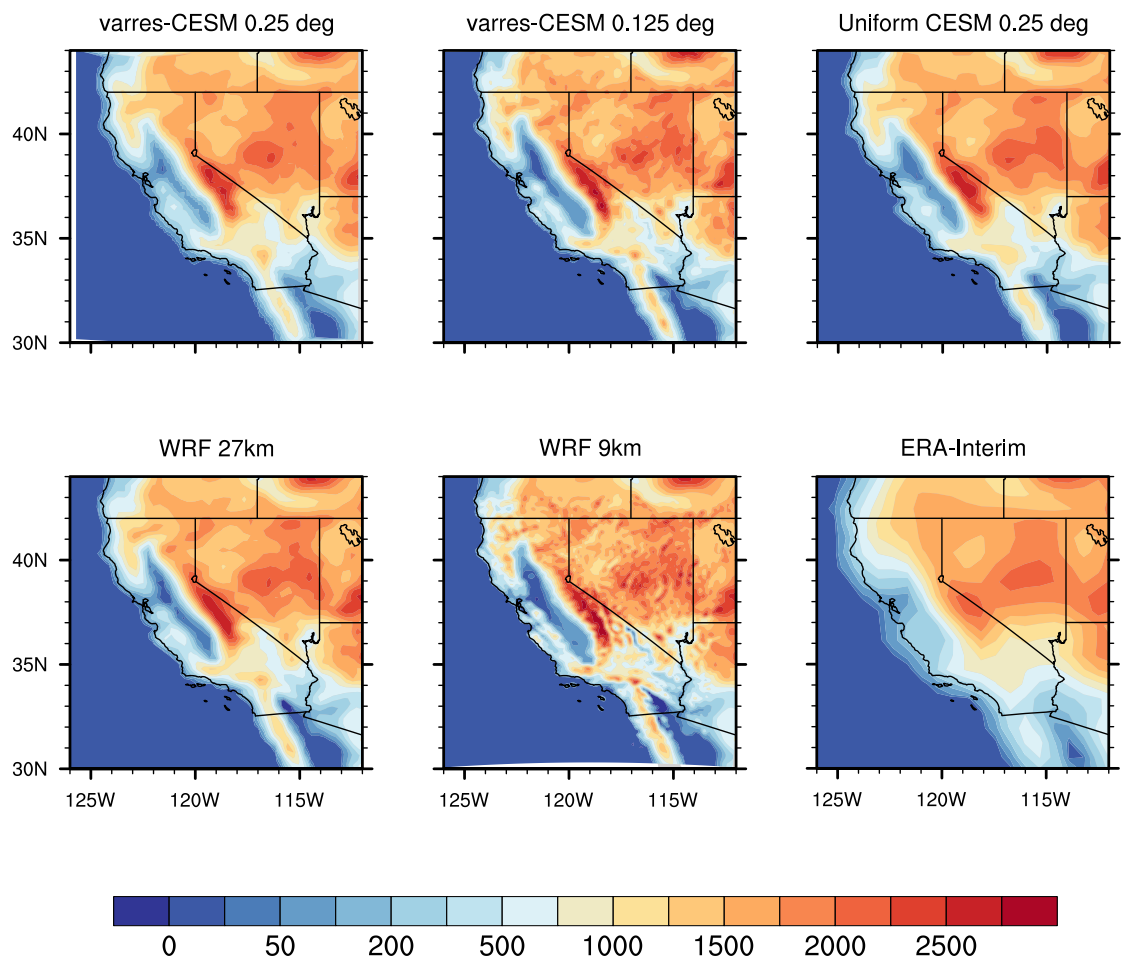
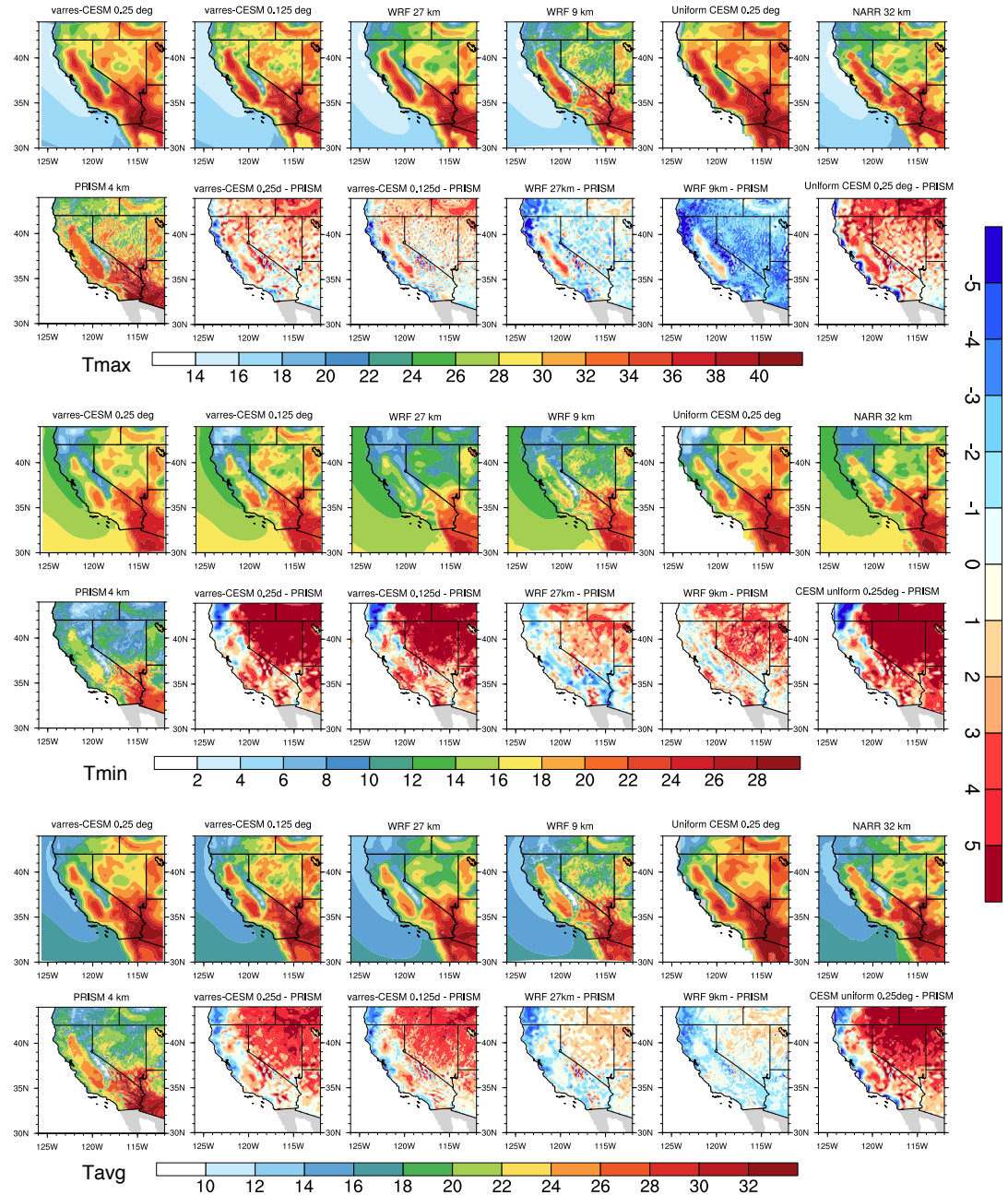


FIG. 2. Grid meshes for the two varres-CESM simulations.



739 FIG. 3. Topography in meters (m) for (top left to bottom right) varres-CESM 0.25° , varres-CESM 0.125° ,
740 uniform CESM-FV 0.25° , WRF 27km, WRF 9km and ERA-Interim (~ 80 km).



741 FIG. 4. JJA average daily Tmax, Tmin and Tavg from models and reference datasets, and differences between
 742 them ($^{\circ}\text{C}$).

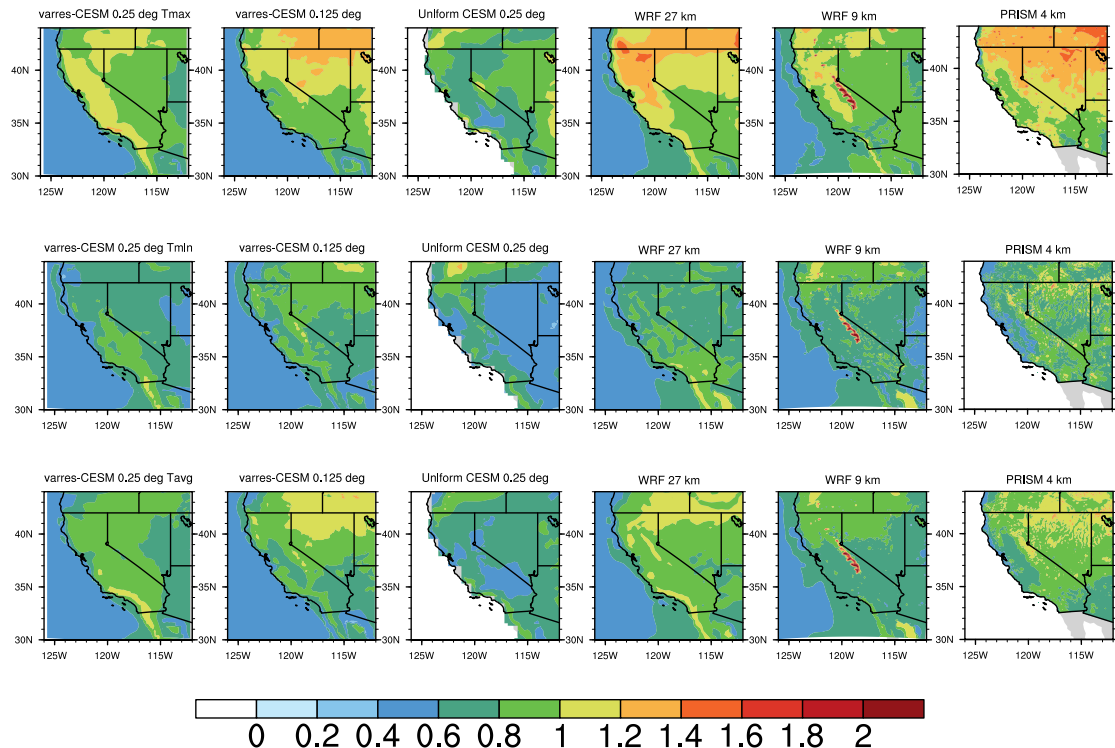
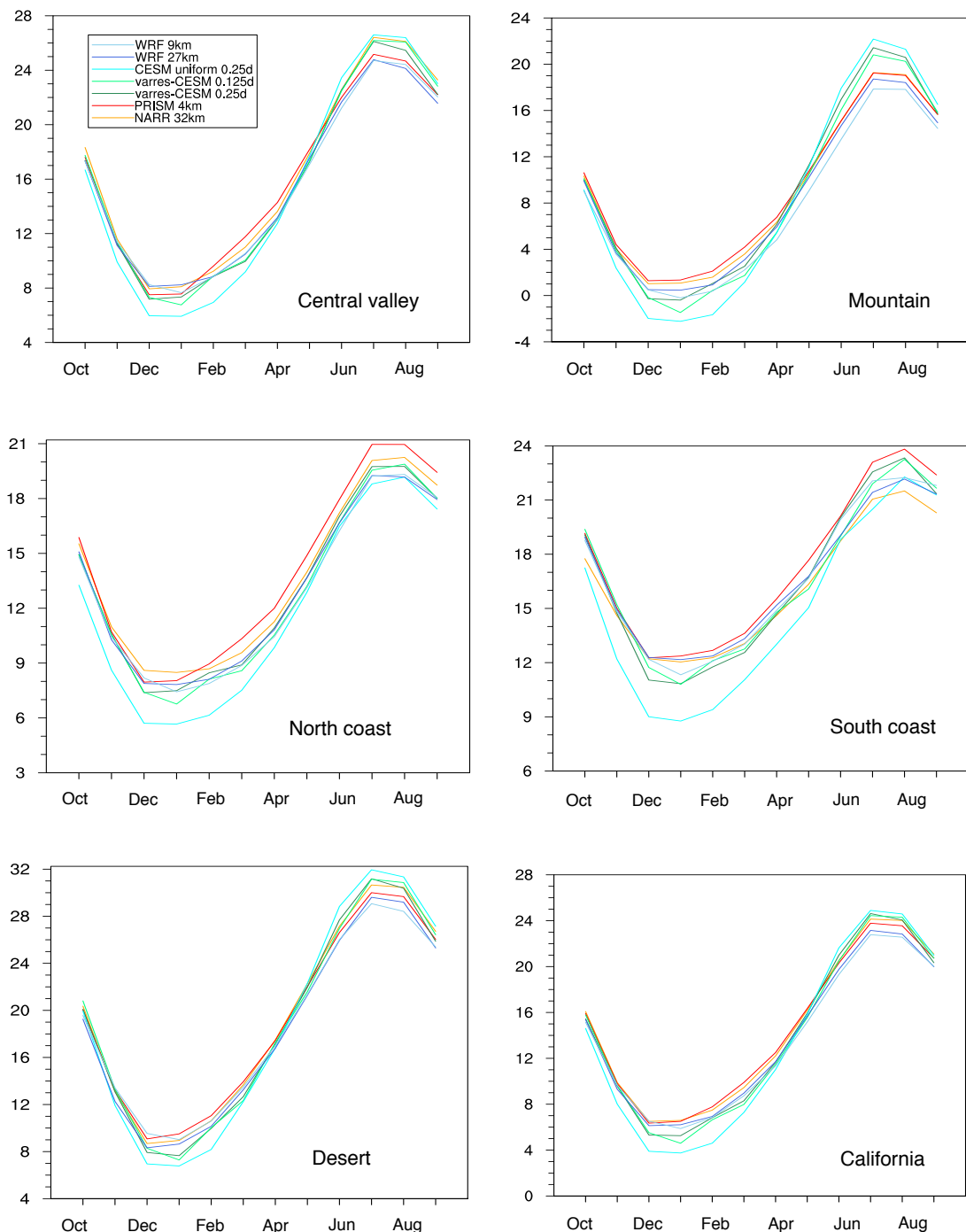
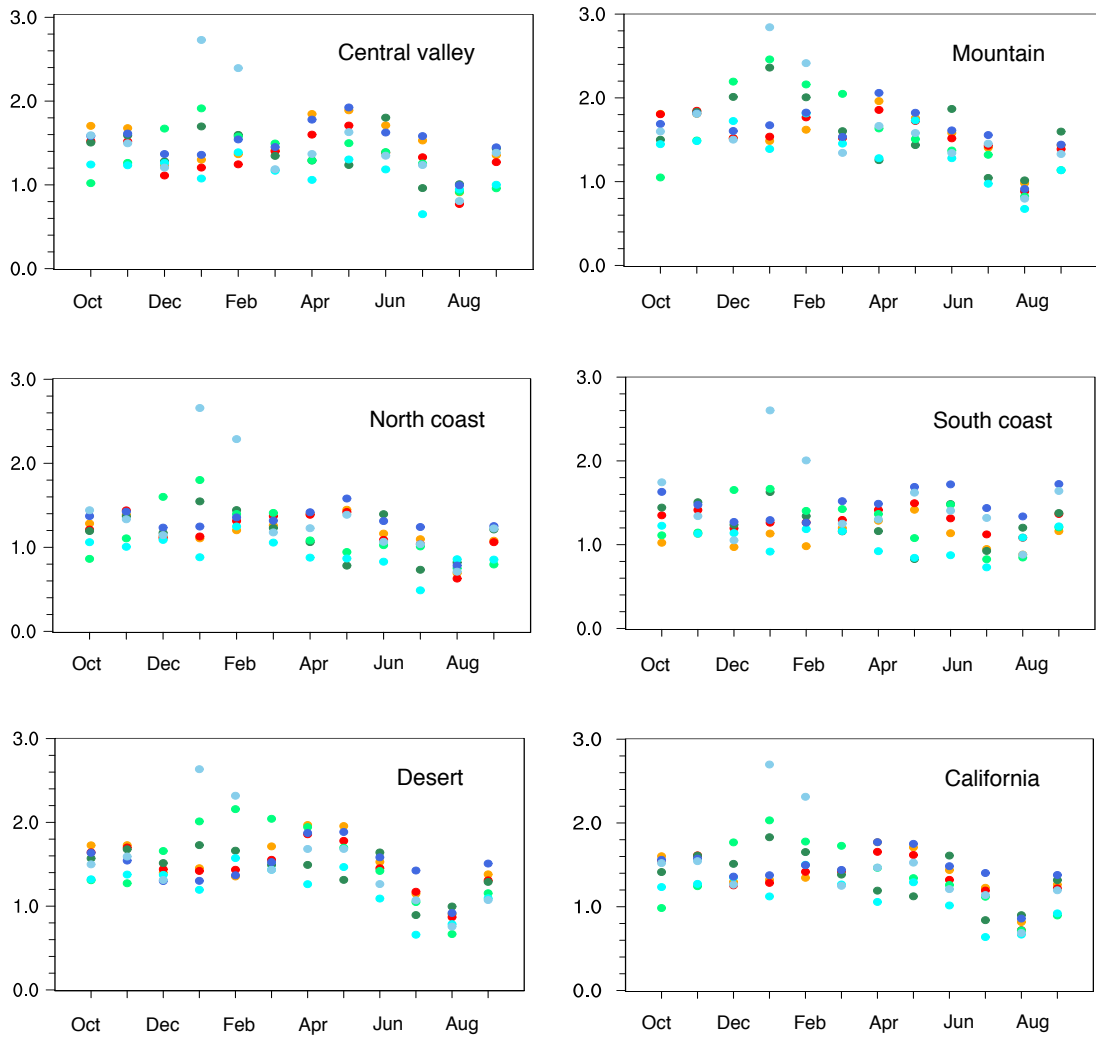


FIG. 5. sample standard deviation of JJA average daily Tmax, Tmin and Tavg from models and PRISM ($^{\circ}\text{C}$).



743 FIG. 6. Seasonal cycle of monthly-average Tavg for each subzone ($^{\circ}\text{C}$). Bars represent standard deviation (σ)
744 values.



745 FIG. 7. Seasonal standard deviation (s) values of monthly-average T_{avg} for each subzone ($^{\circ}C$). Bars represent
746 standard deviation (s) values.

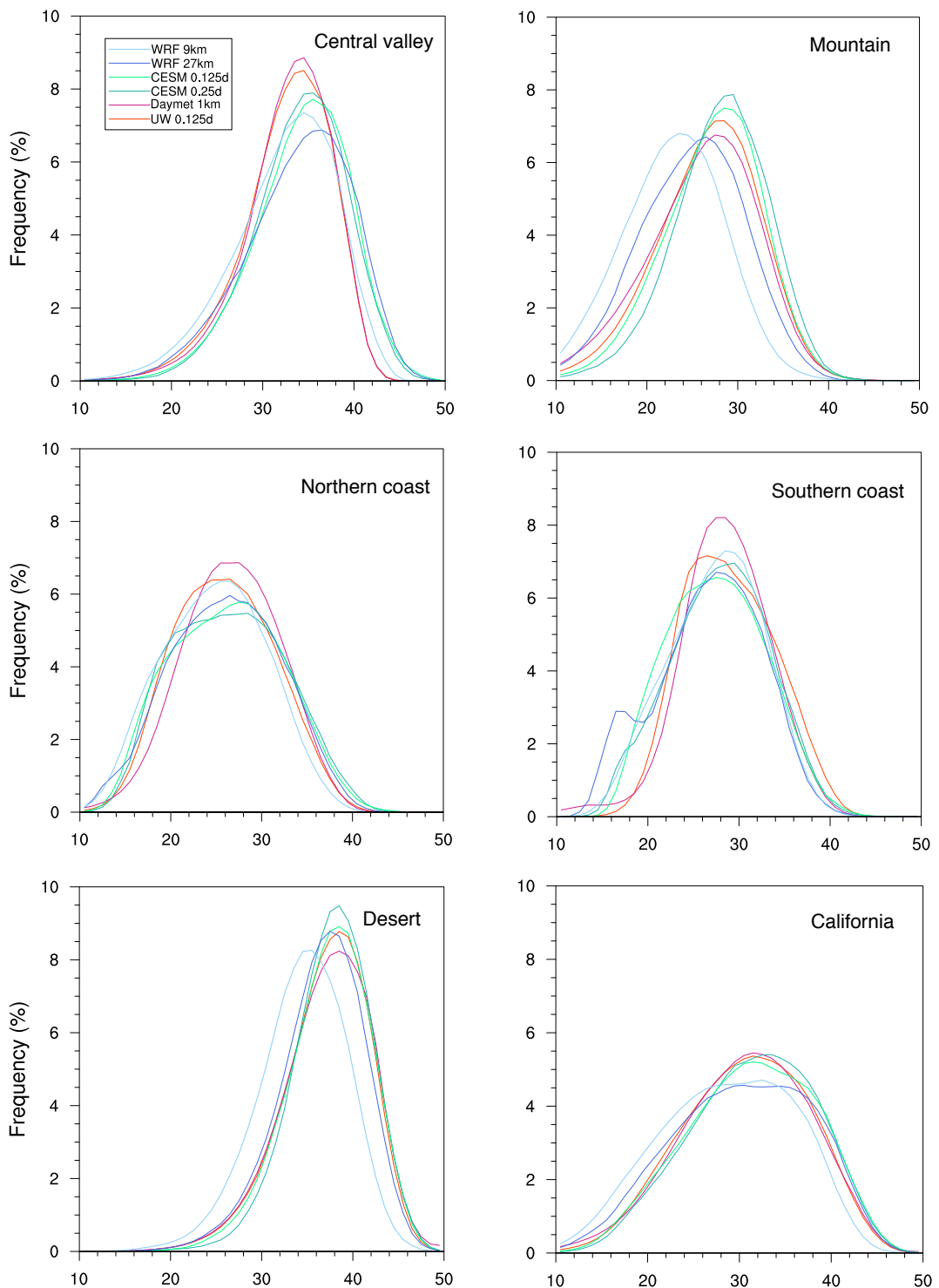


FIG. 8. Frequency distribution of summer Tmax ($^{\circ}\text{C}$).

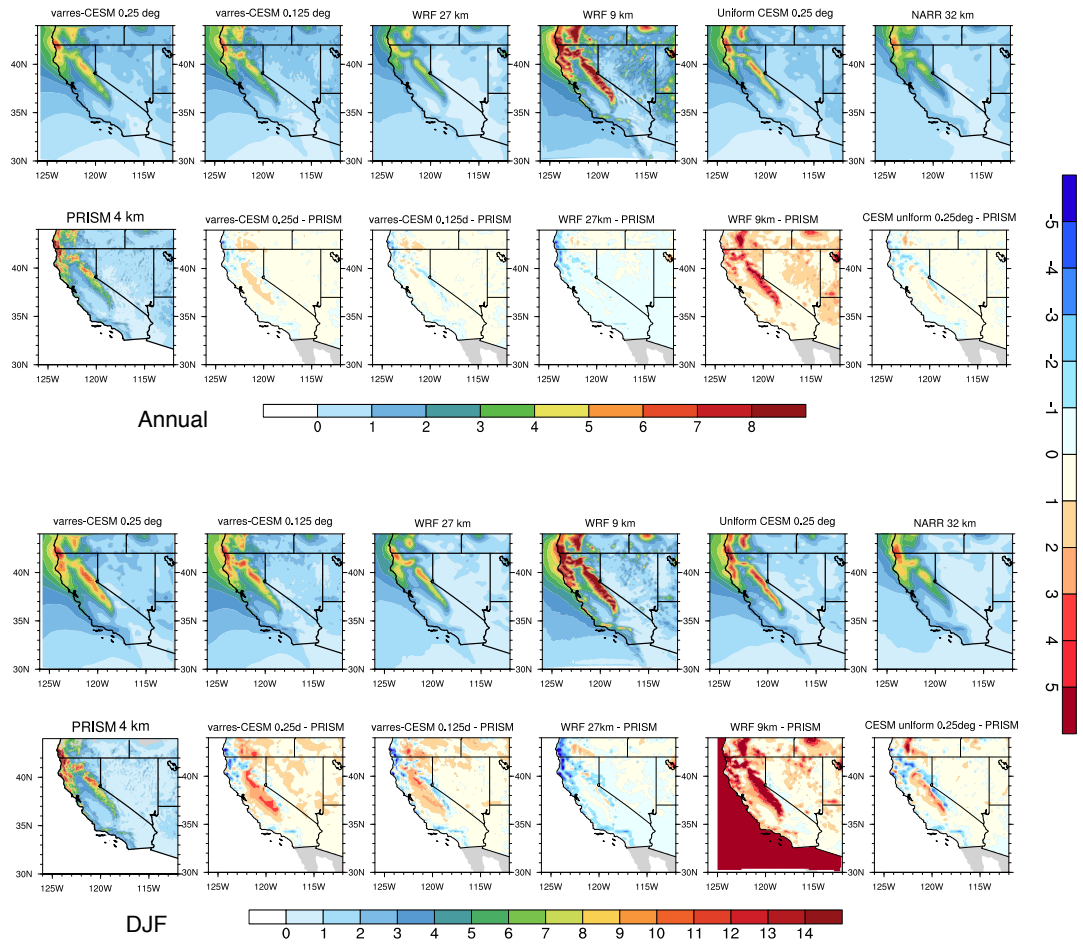


FIG. 9. Annual and DJF precipitation from models and reference datasets (mm/d).

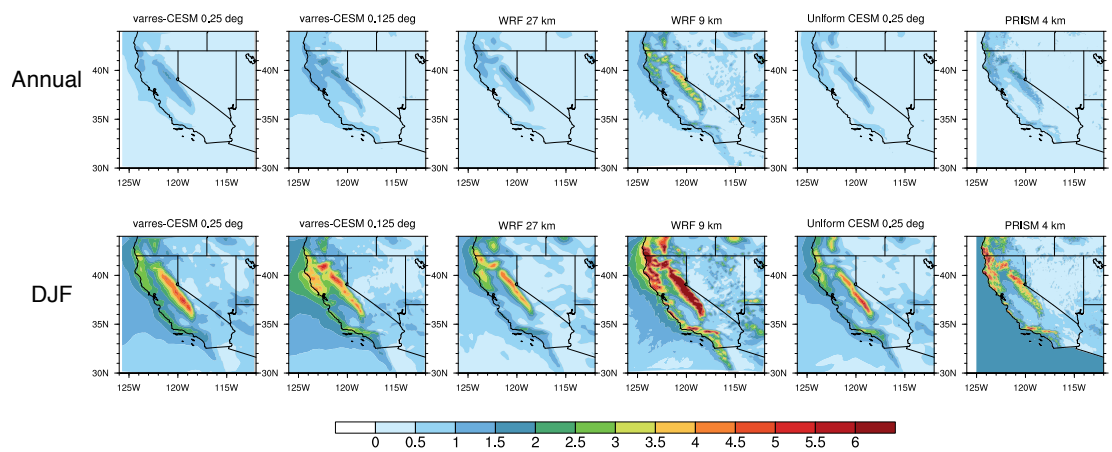


FIG. 10. sample standard deviation of Annual and DJF precipitation from models and PRISM (mm/d).

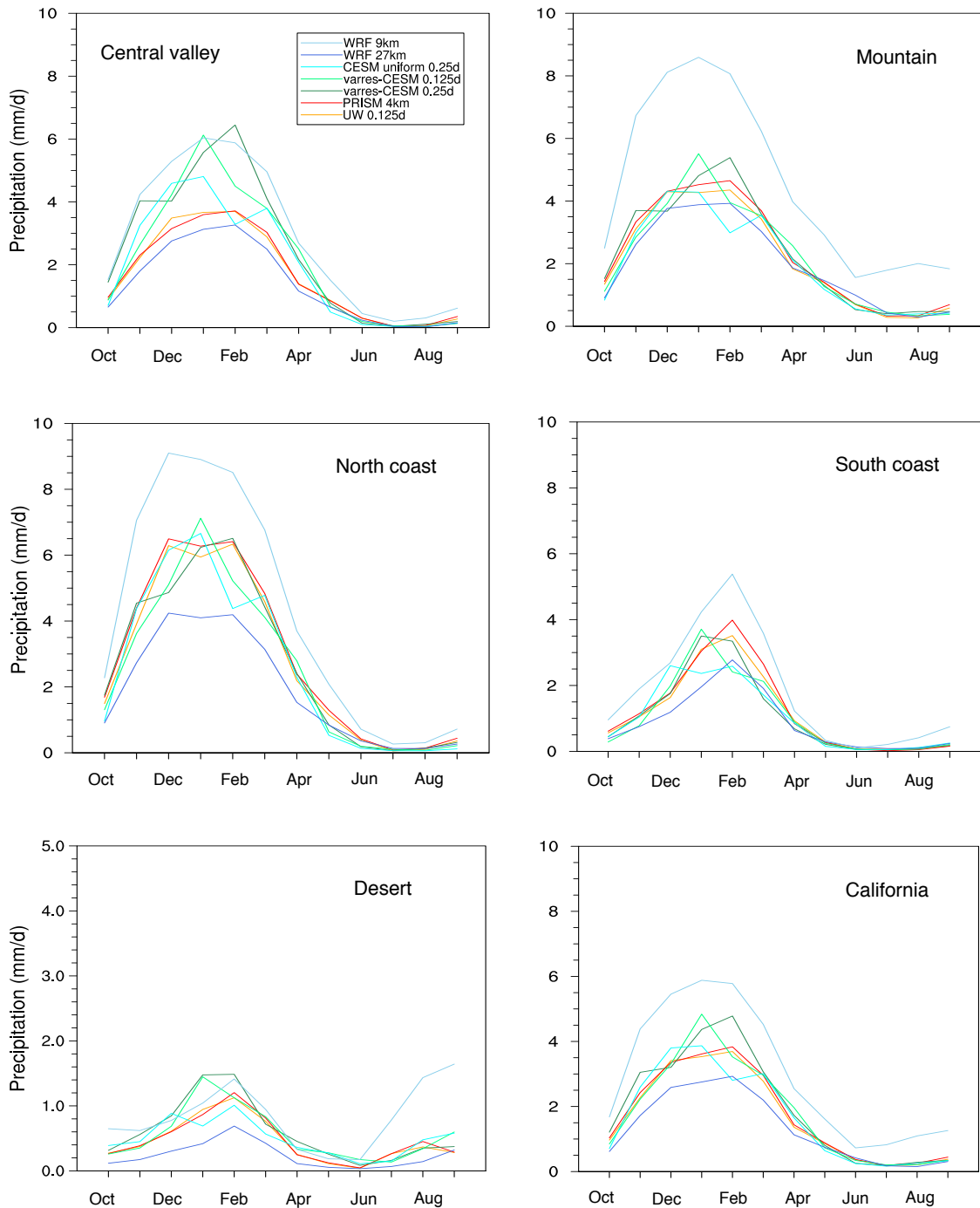


FIG. 11. As Figure 6, but for monthly-average total precipitation (mm/d).

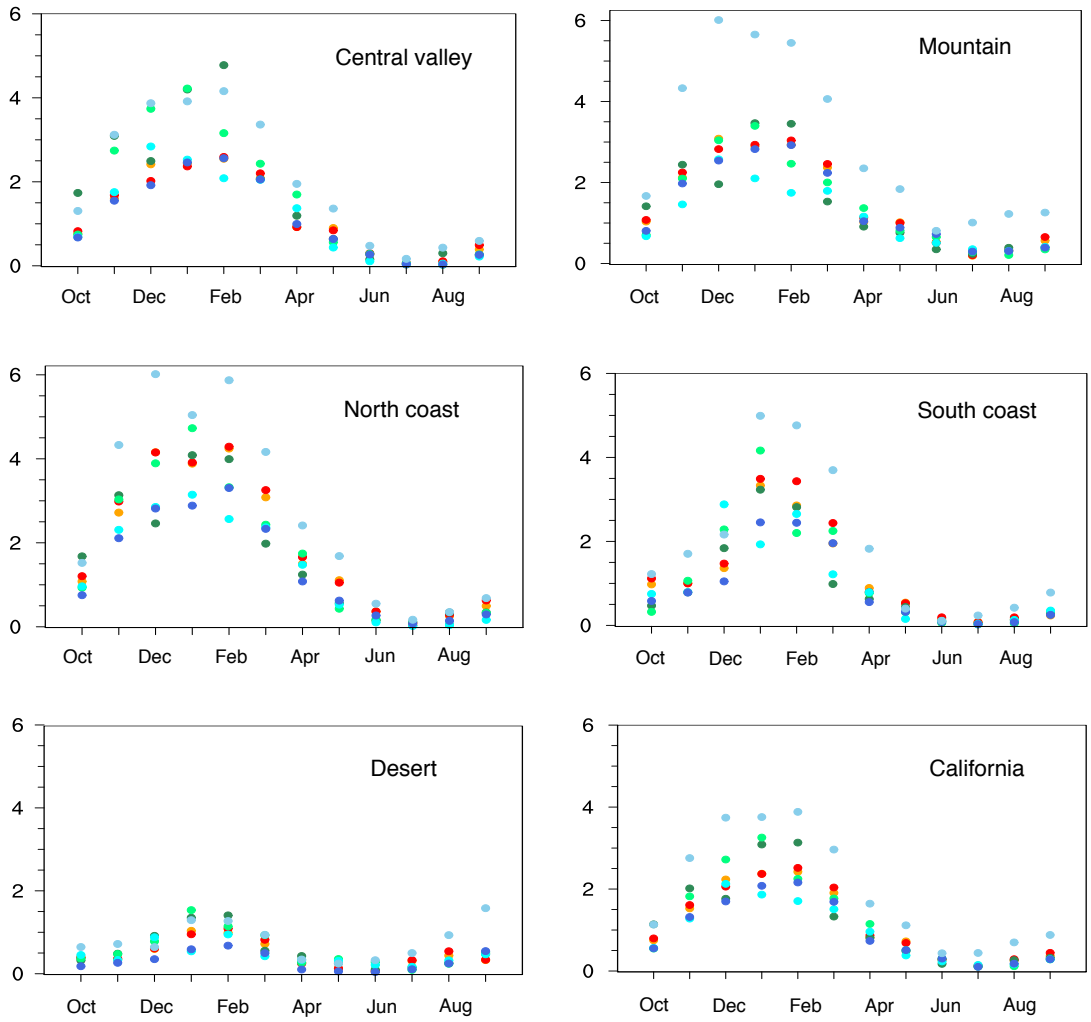
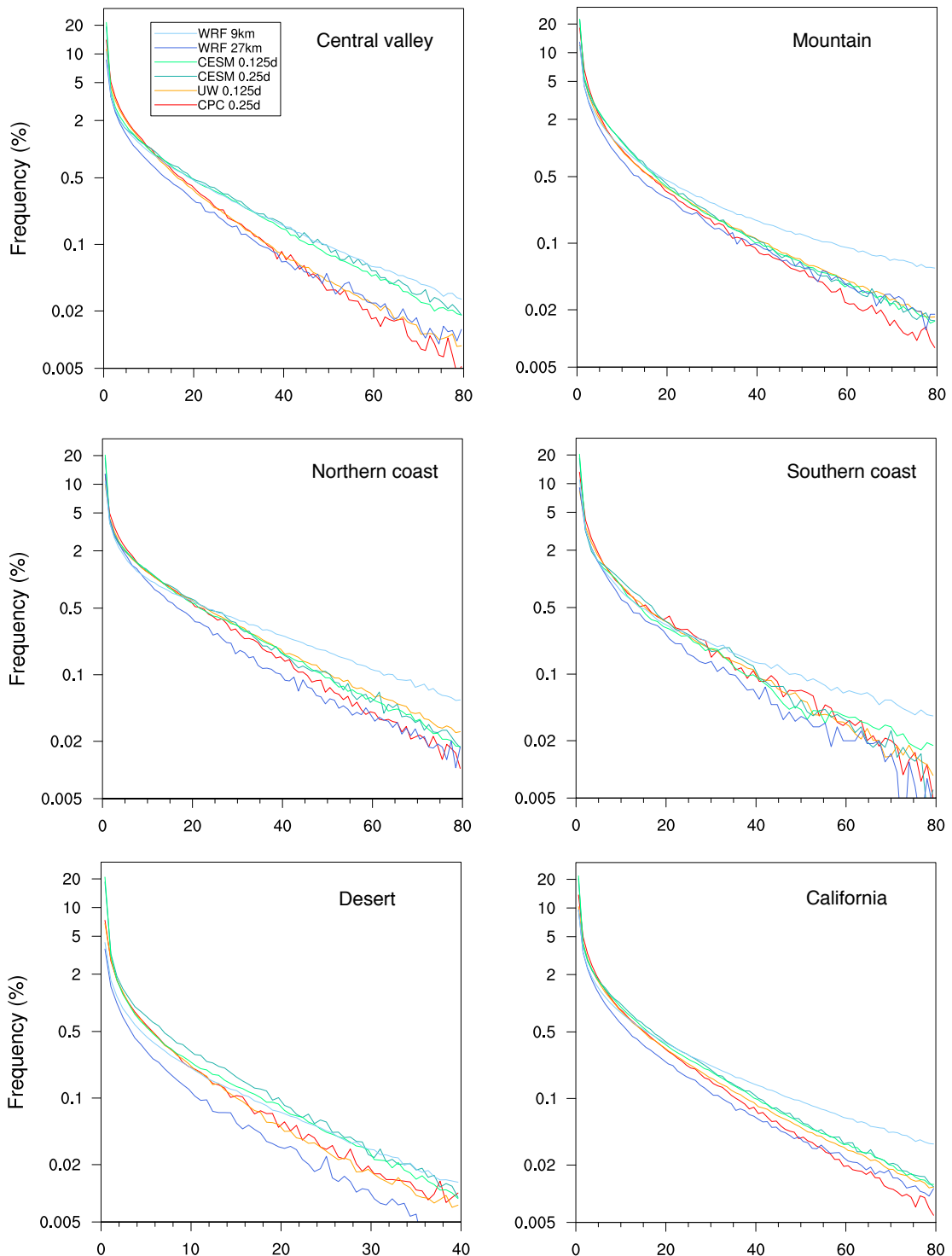
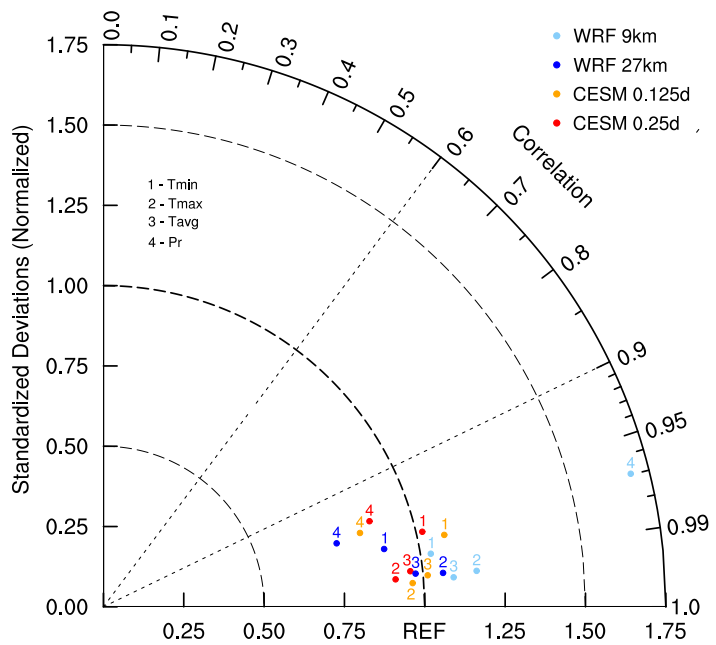


FIG. 12. As Figure 7, but for monthly-average total precipitation (mm/d).



747 FIG. 13. Frequency distribution of winter Pr constructed from 26 years of daily data (mm/d) (note that the
 748 vertical scale is logarithmic).



749 FIG. 14. Taylor diagram of annual climatology for the entire California region, using the PRISM dataset as
 750 reference.